Aminocarbyne-Alkyne Coupling in Diruthenium Complexes: Exploring the Anticancer Potential of the Resulting Vinyliminium Complexes and Comparison with Diiron Homologues

Benedetta Bertoncini, Zhimei Xiao, Stefano Zacchini, Lorenzo Biancalana, Gilles Gasser, Fabio Marchetti

▶ **To cite this version:**

Benedetta Bertoncini, Zhimei Xiao, Stefano Zacchini, Lorenzo Biancalana, Gilles Gasser, et al.. Aminocarbyne-Alkyne Coupling in Diruthenium Complexes: Exploring the Anticancer Potential of the Resulting Vinyliminium Complexes and Comparison with Diiron Homologues. Inorganic Chemistry, 2024, 10.1021/acs.inorgchem.4c01119 . hal-04622509

HAL Id: hal-04622509
https://hal.science/hal-04622509v1

Submitted on 24 Jun 2024

HAL is a multi-disciplinary open access archive for the deposit and dissemination of scientific research documents, whether they are published or not. The documents may come from teaching and research institutions in France or abroad, or from public or private research centers.

L'archive ouverte pluridisciplinaire **HAL**, est destinée au dépôt et à la diffusion de documents scientifiques de niveau recherche, publiés ou non, émanant des établissements d'enseignement et de recherche français ou étrangers, des laboratoires publics ou privés.

Aminocarbyne-Alkyne Coupling in Diruthenium Complexes: Exploring the Anticancer Potential of the Resulting Vinyliminium Complexes and Comparison with Diiron Homologues

Benedetta Bertoncini,[a] Zhimei Xiao,[b] Stefano Zacchini,[c] Lorenzo Biancalana,[a,*] Gilles Gasser,[b,*] Fabio Marchetti [a,*]

[a] University of Pisa, Department of Chemistry and Industrial Chemistry, Via G. Moruzzi 13, I-56124 Pisa, Italy

[b] Chimie ParisTech, PSL University, CNRS, Institute of Chemistry for Life and Health, 11 Rue Pierre et Marie Curie, 75005 Paris, France

[c] University of Bologna, Department of Industrial Chemistry "Toso Montanari", Via P. Gobetti 85, I-40129 Bologna, Italy

Corresponding Authors

lorenzo.biancalana@unipi.it, gilles.gasser@chimieparistech.psl.eu, fabio.marchetti@unipi.it

Abstract

New diruthenium complexes based on the scaffold $Ru_2Cp_2(CO)_2$ (Cp = η^5-C_5H_5) and containing a bridging vinyliminium ligand, [**2a-d**]CF_3SO_3, were synthesized through regioselective coupling of alkynes with an aminocarbyne precursor (85-90 % yields). The reaction involving phenylacetylene proceeded with the formation of a diruthenacyclobutene byproduct, [**4**]CF_3SO_3 (10% yield). Complexes [**2a-d**]$^+$ undergo partial alkyne extrusion in contact with alumina or $CDCl_3$. All products were characterized by elemental analysis, infrared and multinuclear NMR spectroscopy, and single crystal X-ray diffraction in two cases. Complexes [**2a-d**]$^+$ revealed an outstanding stability in DMEM cell culture medium at 37 °C (< 1 % degradation over 72 h). These complexes exhibited cytotoxicity in human colon colorectal adenocarcinoma HT-29 cells in the low micromolar range, with lower IC_{50} values than those obtained with the homologous diiron complexes previously reported. Evaluation of ROS (reactive oxygen species) production and O_2 consumption rate (OCR) highlighted the higher potential of Ru_2 complexes, compared to the Fe_2 counterparts, to impact mitochondrial activity, with the heterometallic Ru_2-ferrocenyl complex [**2d**]$^+$ showing the best performance.

Keywords: Bioorganometallic chemistry, cytotoxicity, reactive oxygen species, ruthenium complexes, vinyliminium ligand.

1. Introduction

Ruthenium complexes have undergone extensive exploration for their potential in anticancer applications,[1,2,3,4] aiming to identify suitable alternatives to platinum-based drugs that are commonly used in hospital chemotherapy treatment.[5,6,7] With respect to platinum species, it is generally accepted that ruthenium offers the advantage of limited toxicity and satisfying tolerability in the human body.[8,9,10] A diversity of ruthenium compounds has been investigated, and a few ruthenium(III) complexes were evaluated, or are still under evaluation, in clinical trials.[11,12,13] These compounds behave as pro-drugs, undergoing monoelectronic reduction of the metal center (from Ru^{III}

to Ru^{II}) within the tumor environments characterized by hypoxic conditions.[14,15] Recognizing the potential of Ru^{II} derivatives, many organo-ruthenium(II) complexes have been examined,[16,17,18] and particularly complexes belonging to the RAPTA family have shown a great promise.[19,20,21,22]

Dinuclear organometallic complexes are featured by cooperative effects supplied by the proximity of two metal centers, working in concert to provide bridging ligands with expanded, uncommon reactivity compared to analogous mononuclear complexes.[23,24,25,26,27] This unique reactivity enables the building of structural motifs with wide variability,[28,29] offering opportunities in bioorganometallic chemistry to identify optimal groups for finely tuning physicochemical properties.[30] The application of this concept extends to diruthenium complexes,[31,32,33,34] and we contributed to this specific field by evaluating the in vitro antiproliferative activity of cationic derivatives of $[Ru_2Cp_2(CO)_4]$ with bridging allenyl-[35] and vinyl-[36] functionalized ligands. Besides, we uncovered the anticancer activity of diiron complexes derived from $[Fe_2Cp_2(CO)_4]$ and comprising bridging aminocarbyne, $[\mathbf{1}^{Fe}]^+$ [37] or vinyliminium ligands, $[\mathbf{2}^{Fe}]^+$.[38,39,40,41,42] The latter class of compounds is obtained from the former through a wide-scope two-step process (> 150 reported examples of diiron vinyliminium complexes).[43] This process consists in the initial replacement of one CO ligand with a labile acetonitrile using the Me_3NO strategy,[44,45,46] followed by the insertion of a selected alkyne into iron-carbyne bond (Scheme 1).

The cytotoxicity of both aminocarbyne and vinyliminium diiron complexes varies according to the nature of the R, R' and R" substituents. Mechanistic studies pointed out that the observed activity is predominantly associated with the ability of the complexes to disrupt mitochondrial redox homeostasis, through the slow disassembly of the organo-diiron scaffold occurring intracellularly. This disassembly results in the liberation of carbon monoxide and, presumably, redox-reactive iron(I) species which rapidly convert into iron(III) derivatives.

Motivated by the parallel chemistry often exhibited by the commercially available, group 8 metal dimers $[M_2Cp_2(CO)_4]$ (M = Fe, Ru),[47,48,49] we recently reported a systematic synthetic study to access a series of Ru_2 homologues of $[\mathbf{1}^{Fe}]^+$, and an evaluation of their in vitro cytotoxicity, revealing a

notable profile.[50] The chemistry of diruthenium μ-vinyliminium complexes has been substantially underdeveloped compared to their diiron homologues [**2**^{Fe}]$^+$, with only 15 examples reported,[51] and their biological applications have not been explored so far.

In this study, we present the straightforward synthesis of a set of diruthenium vinyliminium complexes, starting from the easily available *N*-cyclohexyl compound $[Ru_2Cp_2(CO)_2(\mu\text{-}CO)\{\mu\text{-}CNMe(Cy)\}]CF_3SO_3$, [**1**]$CF_3SO_3$, and we discuss targeted experiments designed for a preliminary evaluation of their anticancer properties. Moreover, a parallel study has been conducted on corresponding diiron complexes, providing a rare literature example of comparative biological evaluation of homologous group 8 metal complexes.[52]

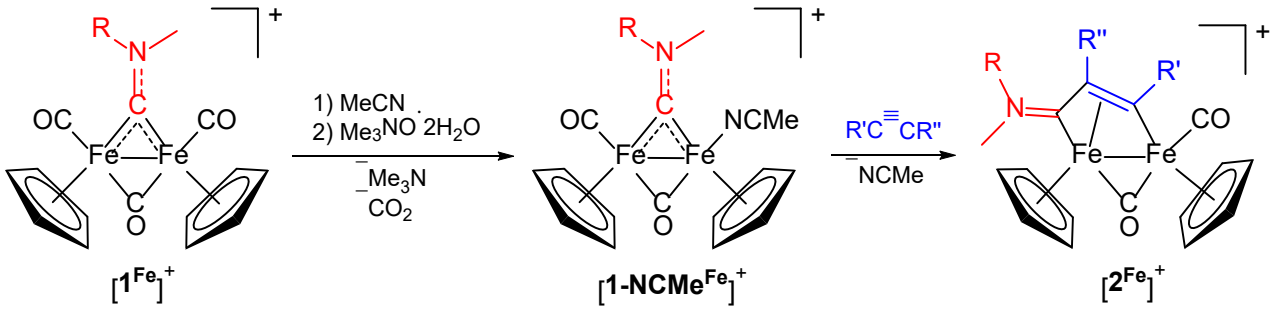

Scheme 1. Diiron μ-aminocarbyne complexes, [**1**^{Fe}]$^+$, and their two-step transformation into μ-vinyliminium complexes, [**2**^{Fe}]$^+$, through the coupling of aminocarbyne ligand (red) with alkynes (blue). R = alkyl or aryl; R′ = H, alkyl, aryl, thiophenyl, pyridyl, silyl, carboxylate; R″ = H (most frequently), Me, Et, carboxylate.

2. Results and discussion

2.1 Synthesis and structural characterization of diruthenium complexes.

Based on the wide-scope route to access diiron vinyliminium complexes (Scheme 1), $[Ru_2Cp_2(CO)_2(\mu\text{-}CO)\{\mu\text{-}CNMe(Cy)\}]CF_3SO_3$, [**1**]$CF_3SO_3$, was treated with trimethylamine *N*-oxide in acetonitrile, resulting in the formation of $[Ru_2Cp_2(NCMe)(CO)(\mu\text{-}CO)\{\mu\text{-}CNMe(Cy)\}]^+$, [**1-NCMe**]$^+$ (Scheme 2a). However, [**1-NCMe**]$^+$ exhibited gradual decomposition in organic solvents yielding a mixture of unidentified products, and the subsequent reactions with a selection of alkynes in various conditions were unsatisfactory in terms of conversion and selectivity (Scheme 2b). Consequently, an optimized one-pot procedure was developed involving the treatment of [**1**]CF_3SO_3

with an excess of trimethylamine *N*-oxide and the selected alkyne, working at room or reflux temperature depending on the volatility of the alkyne (Scheme 2c). Almost quantitative formation of the desired μ-vinyliminium species $[Ru_2Cp_2(CO)(\mu\text{-}CO)\{\mu\text{-}\kappa C\text{:}\eta^3\text{-}C^3(R')C^2(R'')C^1NMe(C_6H_{11})\}]^+$,[53] [**2a-d**]$^+$, was achieved with propyne, 2-butyne, phenylacetylene and ethynylferrocene. Washing the crude reaction mixture with diethyl ether/hexane mixtures allowed to isolate the corresponding triflate salts as dark brown ([**2a-b**]$^+$) or orange-red ([**2c-d**]$^+$) air-stable solids in 85-90 % yield.

Unlike the purification method used for the diiron counterparts,[51] alumina chromatography is unsuitable for [**2a-d**]CF_3SO_3 as it induces partial conversion of the μ-vinyliminium products into the chlorido μ-aminocarbyne derivative $[Ru_2Cp_2Cl(CO)(\mu\text{-}CO)\{\mu\text{-}CNMe(Cy)\}]$, **3**. Formation of **3** was also observed in $CDCl_3$ solutions of [**2a-d**]CF_3SO_3 left at room temperature for hours. These reactions (Scheme 2d) involve the disassembly of the μ-vinyliminium ligand through alkyne de-insertion and the addition of chloride from either the chlorinated solvent or NaCl present in commercial alumina. Compound **3** was directly prepared from [**1**]CF_3SO_3 by treatment with excess LiCl in refluxing isopropanol and isolated as an orange solid in 87 % yield following alumina chromatography (Scheme 2e).

While [**2a**,**b**,**d**]CF_3SO_3 were selectively formed and isolated as pure compounds, we noticed that the reaction of [**1**]$^+$ with phenylacetylene reproducibly afforded a minor (8-11 %) organometallic by-product, [**4**]$^+$, which could not be easily separated from [**2c**]$^+$. Nevertheless, we successfully purified [**4**]$^+$ from [**2c**]$^+$, by taking advantage of the long-term instability of the latter on alumina (see above). Thus, the crude reaction mixture was dissolved in a few milliliters of THF and applied to the top of an alumina column. After 9 days at room temperature, a red band was eluted from which [**4**]CF_3SO_3 was obtained as a red solid in low yield (Scheme 2f). Based on spectroscopic and spectrometric evidence (*vide infra*), [**4**]$^+$ differs from [**2c**]$^+$ due to a bridging phenylethene-1,2-diyl ligand (μ-κC^1:κC^2-PhC=CH) in place of the bridging carbonyl. Related structures containing a 1,2-diruthena-3,4-cyclobutene fragment were previously obtained from $[Ru_2Cp^X{}_2(CO)_4]$ ($Cp^X = C_5H_4^-$, $[C_5H_4\text{-}C_5H_4]^{2-}$, $[C_5H_4(CH_2)C_5H_4]^{2-}$ or $[C_5H_3(SiMe_2)_2C_5H_3]^{2-}$) and alkynes under photolytic conditions.[54,55,56,57,58]

Attempts to obtain $[\mathbf{4}]^+$ by reaction of $[\mathbf{2c}]^+$, phenylacetylene and various Lewis acids or bases were not successful (see ESI for details). Slow addition of PhCCH and Me_3NO to a $[\mathbf{1}]^+$ solution in ^{i}PrOH at – 20 °C led to a mixture of products including $[\mathbf{2c}]^+$ but not $[\mathbf{4}]^+$. Instead, under harsher conditions (5.0 eq. of PhCCH and Me_3NO, refluxing isopropanol, 16 h) the relative amount of $[\mathbf{4}]^+$ in the mixture increased ($[\mathbf{2c}]^+/[\mathbf{4}]^+$ ratio = 4.2). These results indicate that $[\mathbf{4}]^+$ is not a kinetic product of the $[\mathbf{1}]^+/Me_3NO/PhCCH$ interaction.

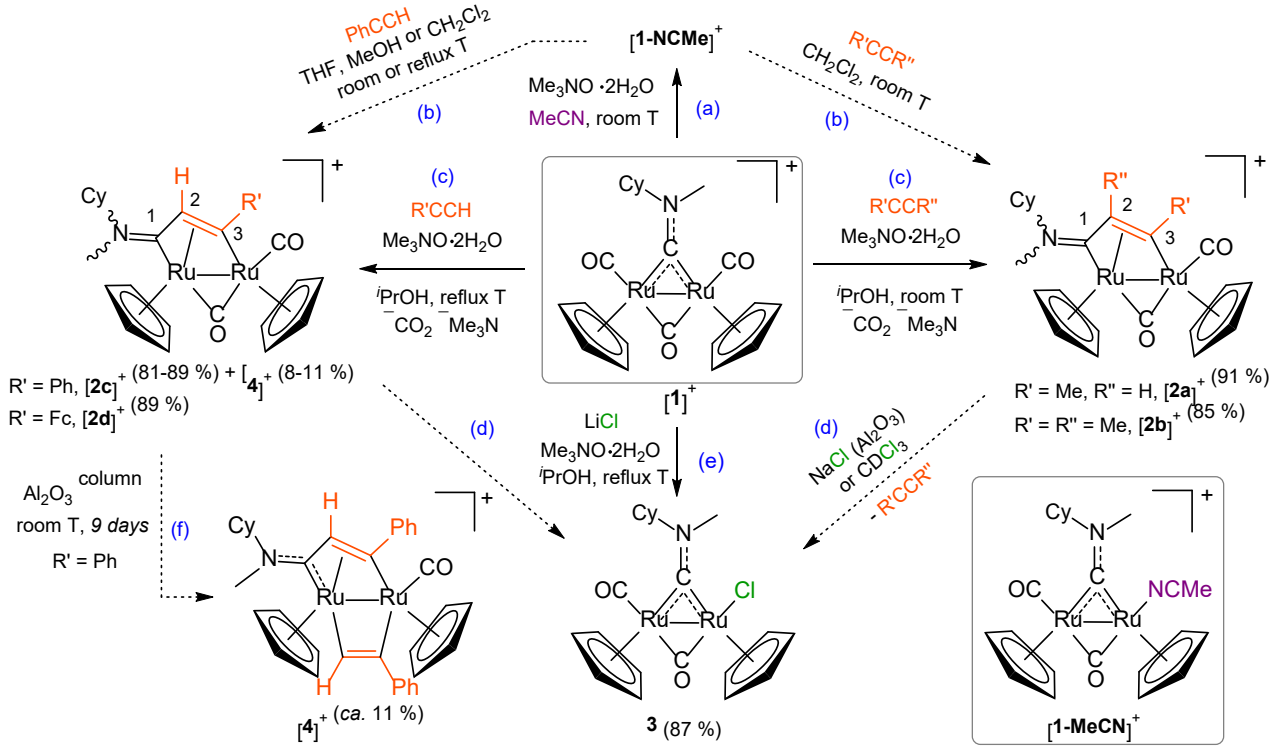

Scheme 2. Formation of the acetonitrile μ-aminocarbyne complex $[\mathbf{1a\text{-}NCMe}]^+$ from the tricarbonyl precursor $[\mathbf{1}]^+$ (**a**) and subsequent alkyne insertion (**b**). One-pot procedure for the preparation of diruthenium μ-vinyliminium complexes $[\mathbf{2a\text{-}d}]^+$ from $[\mathbf{1}]^+$/alkyne/Me_3NO (**c**). Incidental formation of the chlorido μ-aminocarbyne complex **3** from the μ-vinyliminium complexes (**d**) and direct preparation of **3** from $[\mathbf{1}]^+$/LiCl/Me_3NO (**e**). Isolation of the μ-vinyliminium μ-ethene-1,2-diyl complex $[\mathbf{4}]^+$, by-product in the synthesis of $[\mathbf{2c}]^+$ (**f**). Dashed lines indicate incomplete reactions / non-preparative routes. Triflate as counteranion for cationic complexes; isolated yield in parentheses. Cy = C_6H_{11}, cyclohexyl; Fc = η^4-C_5H_4FeCp, ferrocenyl. Numbering refers to carbon atoms.

The unprecedented compounds $[\mathbf{2a\text{-}d}]CF_3SO_3$ and **3** were characterized by elemental (CHNS) analyses, IR and NMR spectroscopy (Figures S1-S18). The stereochemistry in solution was assigned based on previous studies on related complexes.[51] Specifically, the orientation of the *N*-substituents around the iminium group and that of the cyclopentadienyl ligands with respect to the $Fe_2(\mu\text{-}CO)(\mu$-

C) core may give rise to *E*/*Z* and *cis*/*trans* isomerism, respectively. Importantly, the insertion of terminal alkynes takes place in a fully regioselective mode, positioning the substituent R' far from the iminium moiety.

The IR spectra of [**2a-d**]$^+$ in dichloromethane exhibit diagnostic bands at 1984–1992 and 1816–1820 cm^{-1} for the terminal and bridging carbonyls, respectively, and at 1651–1662 cm^{-1} for the iminium group. The carbonyl stretching vibrations are shifted to lower wavenumbers (− 15-20 cm^{-1}) in the solid state. The ^{1}H and ^{13}C NMR spectra of [**2a-d**]CF_3SO_3 show two sets of resonances of comparable intensities (1.1 to 1.4 ratio), indicative of *cis*-*E*/*Z* isomers. The major isomer for [**2a**]$^+$ and [**2c**]$^+$ displays the cyclopentadienyl ligand and *N*-cyclohexyl group next to each other (*Z* stereochemistry) while the opposite situation (*E* stereochemistry for the major isomer) occurs for [**2b**]$^+$ and [**2d**]$^+$. The stereochemistry of [**2c**]$^+$ was confirmed by ^{1}H NOESY experiments, upon selective irradiation of a cyclopentadienyl ligand (Figure S11). The *Z*/*E* isomer ratios observed for the sub-zero or room temperature preparations of [**2c**]$^+$, as well as that after 16 h under refluxing isopropanol (1.0, 1.3 and 2.2, respectively), indicate that *cis*-*Z*-[**2c**]$^+$ is thermodynamically more stable and that the *E* to *Z* isomerization process is accessible at *ca.* 80 °C. In addition, two minor sets of signals (5-10 %) are present for [**2d**]$^+$, attributed to *trans*-*E*/*Z* isomers. The carbons of the bridging vinyliminium ligand resonate at 215, 60-72 and 182-188 ppm for C^1, C^{2}H/C^{2}Me and C^3, respectively (Scheme 2). Furthermore, the structure of *cis*-*E*-[**2d**]$^+$ was ascertained by X-ray diffraction (Figure 1). Salient bonding parameters reveal the substantial double bond nature of C(1)-N(1), and a significant electronic delocalization within the C(1)-C(2)-C(3) chain.

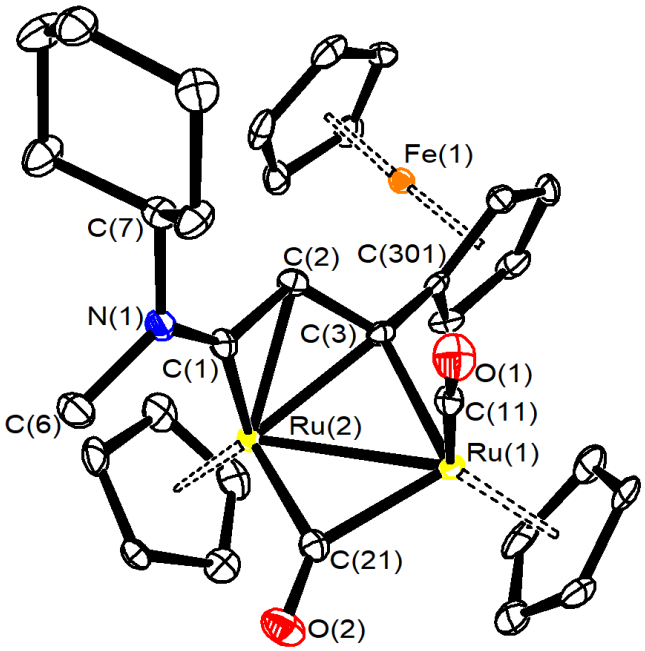

Figure 1. View of the X-ray structure of *cis*-*E*-[**2d**]$^{+}$ ($CF_3SO_3^-$ salt). Displacement ellipsoids are at the 50% probability level. H-atoms have been omitted for clarity. Main bond distances (Å) and angles (°): Ru(1)-Ru(2) 2.7394(6), Ru(1)-C(11) 1.882(5), Ru(1)-C(21) 2.005(5), Ru(2)-C(21), Ru(1)-C(3) 2.065(5), Ru(2)-C(3) 2.169(5), Ru(2)-C(2) 2.188(5), Ru(2)-C(1) 1.961(5), C(11)-O(1) 1.127(6), C(21)-O(2) 1.174(6), C(1)-N(1) 1.290(6), C(1)-C(2) 1.423(7), C(2)-C(3) 1.413(7), Ru(1)-C(11)-O(1) 176.5(5), Ru(1)-C(21)-Ru(2) 84.87(19), Ru(1)-C(3)-Ru(2) 80.58(16), C(1)-C(2)-C(3) 116.9(4), N(1)-C(1)-C(2) 135.2(4), C(1)-N(1)-C(6) 119.1(4), C(1)-N(1)-C(7) 122.1(4), C(6)-N(1)-C(7) 118.5(4).

Compound **3** is featured by two strong carbonyl stretching bands at 1972 and 1796 cm^{-1} (CH_2Cl_2) and a downfield-shifted ^{13}C NMR resonance ($CDCl_3$) at *ca*. 315 ppm for the carbyne carbon. Two sets of signals are present in the ^{1}H and ^{13}C NMR spectra, corresponding to *cis*-*E* and *cis*-*Z* isomers (1.3 ratio). The major isomer in solution (*E*) places the bulky cyclohexyl group and the chloride ligand on opposite sides. The structure of **3** was confirmed by X-ray diffraction (Figure 2).

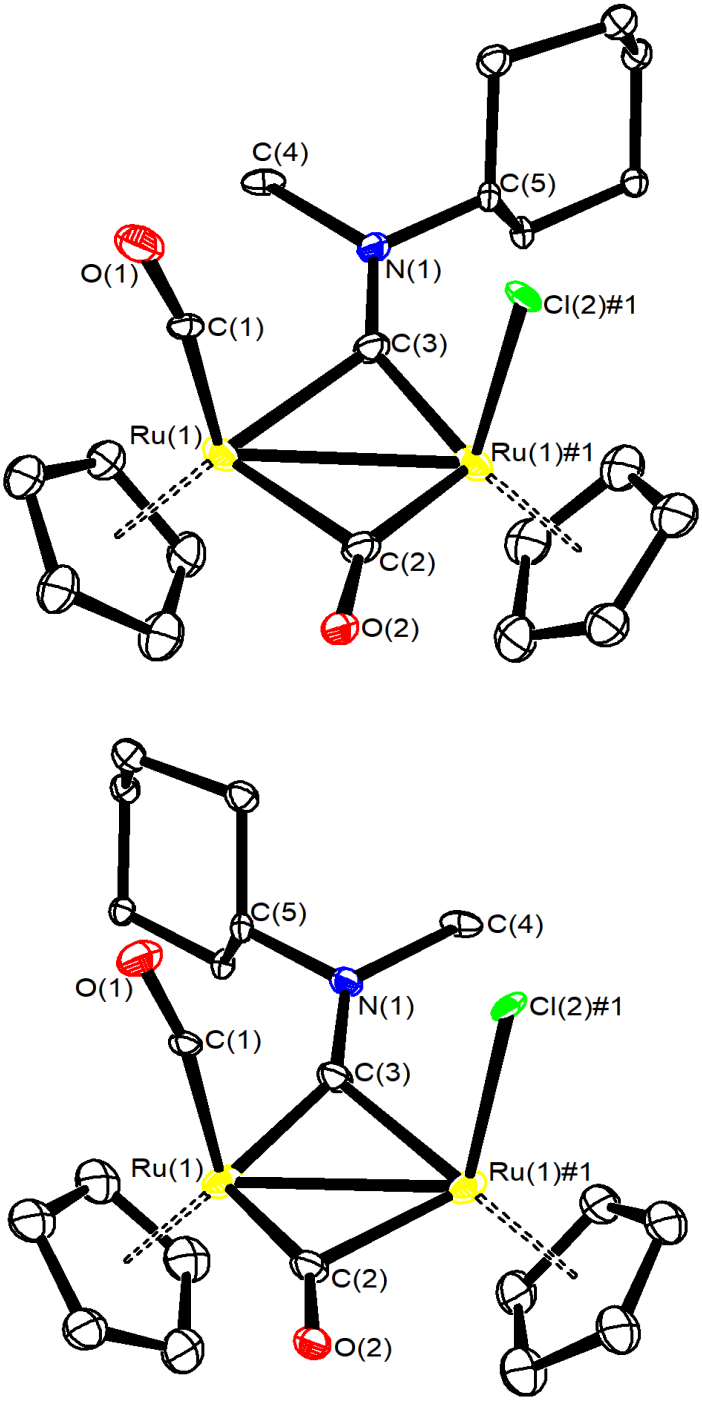

Figure 2. View of the X-ray structure of *cis*-**3**. Displacement ellipsoids are at the 50% probability level. H-atoms have been omitted for clarity. The molecule is disordered and, likely, both *E* and *Z* isomers are present in the solid state. Main bond distances (Å) and angles (°): Ru(1)-Ru(1)#1 2.702(3), Ru(1)-C(1) 1.87(5), Ru(1)#1-Cl(2)#1 2.444(13), Ru(1)-C(2) 1.88(4), Ru(1)#1-C(2) 2.20(4), Ru(1)-C(3) 2.08(4), Ru(1)#1-C(3) 1.82(3), C(1)-O(1) 1.16(5), C(2)-O(2) 1.20(5), C(3)-N(1) 1.34(5) , Ru(1)-C(1)-O(1) 168(4), Ru(1)-C(2)-Ru(1)#1 83(4), Ru(1)-C(3)-Ru(1)#1 87(3), C(3)-N(1)-C(4) 124(3), C(3)-N(1)-C(5) 118(3), C(4)-N(1)-C(5) 118(3). Symmetry transformation used to generate equivalent atoms: #1 -x+1/2, -y+3/2, z.

Compound [**4**]CF_3SO_3 was characterized in solution by IR and NMR spectroscopy and by high resolution mass spectrometry (Figures S19-S23). Selected IR and NMR data for [**4**]$^+$ and [**2c**]$^+$ are

compared in Figure 3. The IR spectrum of $[\mathbf{4}]^+$ in CH_2Cl_2 is featured by a strong absorption at 1996 cm^{-1} for the carbonyl ligand and the lack of bands in the typical C=N range, suggesting a decreased carbon-nitrogen bond order. Accordingly, a single set of signals is present in the ^1H and ^{13}C NMR spectra. Therefore, it is likely that $[\mathbf{4}]^+$ exists as a single isomer in solution due to the combined *cis* orientation of the cyclopentadienyl rings, imposed by the C_2 and C_3 bridging ligands, and the absence of *E*/*Z* isomerism due to free rotation around the C-N moiety. On going from $[\mathbf{2c}]^+$ to $[\mathbf{4}]^+$, the ^1H and ^{13}C NMR resonances for the CH group of the bridging C_3 ligand become significantly deshielded (+ 1.2 and + 9 ppm, respectively), while the ^{13}C NMR signal of the RuCN group moves 14 ppm upfield. The bridging C_2 ligand is characterized by diagnostic ^{13}C NMR resonances around 100 and 110 ppm as well as by a singlet at 6.7 ppm in the ^1H NMR spectrum, evidencing a significant alkenyl character.

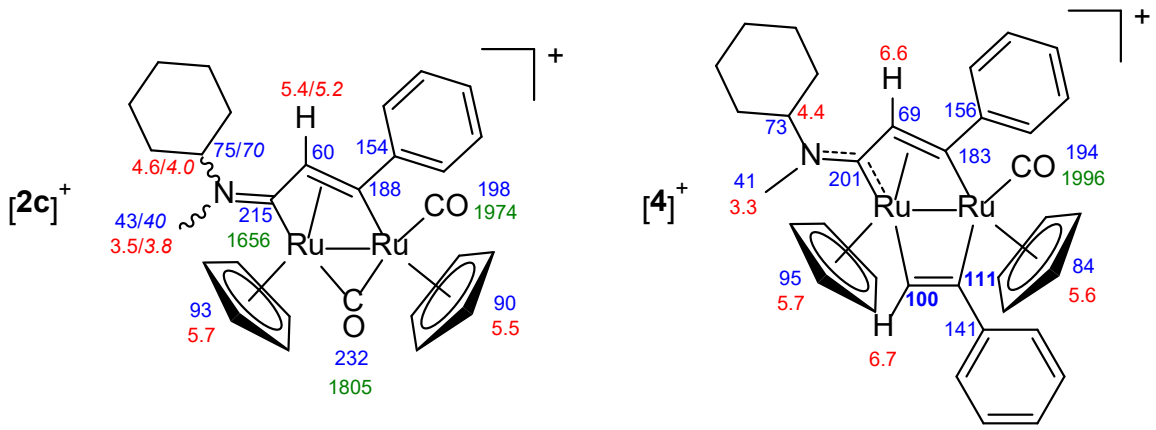

Figure 3. Compared IR (green) absorptions (cm^{-1}), ^1H NMR (red) and ^{13}C NMR (blue) chemical shifts (ppm) for $[\mathbf{2c}]^+$ and $[\mathbf{4}]^+$ ($CF_3SO_3^-$ salts). IR data in CH_2Cl_2; NMR data in $CDCl_3$ for $[\mathbf{2c}]^+$ (major/*minor* isomer only when significantly different), in acetone-d_6 for $[\mathbf{4}]^+$. ^1H NMR data rounded to 0.1 ppm, ^{13}C NMR data rounded to 1 ppm.

2.2 Behavior in aqueous solutions.

The solubility in water (D_2O) and the octanol/water partition coefficient of $[\mathbf{2a\text{-}d}]CF_3SO_3$ were assessed by ^1H NMR and UV-vis spectroscopy, respectively, following established literature methods.[38,37] Additionally, the stability of $[\mathbf{2a\text{-}d}]^+$ in deuterated aqueous solution and in cell culture medium (Dulbecco's Modified Eagle Medium, DMEM) at 37 °C was monitored over a 72 h period by ^1H NMR. Methanol was used as a co-solvent for these experiments, with the percentage ratio

determined by the aqueous solubility of the compounds. The results are summarized in Table 1, along with data for the corresponding diiron counterparts [**2a-d**^{Fe}]CF_3SO_3.

The solubility and Log P_{ow} values of [**2a-d**]CF_3SO_3 are affected by the substituents on the bridging vinyliminium ligand (R, R' in Scheme 1), as expected. Thus, [**2a-b**]CF_3SO_3, with millimolar solubility in D_2O, exhibit a Log P_{ow} of 1.2-1.3, while phenyl- and ferrocenyl-substituted [**2c-d**]CF_3SO_3 are less soluble and more lipophilic. Interestingly, the diruthenium complexes [**2a-d**]CF_3SO_3 are slightly less soluble in water but considerably more lipophilic than the corresponding diiron homologues. Another striking difference between Fe_2 and Ru_2 complexes is represented by the thermal stability under physiological-like conditions. In fact, [**2a-d**]$^+$ (as well as [**4**]$^+$ present together with [**2c**]$^+$, *vide supra*) were totally unchanged after 72 h at 37 °C in both aqueous solution and cell culture medium (^{1}H NMR spectra in Figures S24-S27). Conversely, the diiron complexes experienced a slow, partial (3-22 %) disassembly over 72 h at 37 °C with the eventual formation of iron oxide(s).[38,40,41] Similar trends were previously observed for diruthenium μ-aminocarbyne complexes.[47]

The *E*/*Z* isomer ratios of [**2a-d**]$^+$ remained constant throughout the experiment, consistent with previous findings.[51] The fraction of *trans* isomers of [**2d**]$^+$ in the water/methanol solutions is markedly reduced (≤ 1 %) compared to $CDCl_3$ or acetone-d_6, reflecting their lower solubility in the aqueous medium.

Table 1. Solubility in water (D_2O), octanol/water partition coefficients (Log P_{ow}) and thermal stability in aqueous and cell culture medium solution of diruthenium vinyliminium compounds [**2a-d**]CF_3SO_3 and their diiron counterparts [**2a-2d**^{Fe}]CF_3SO_3 (in *italics*).

Compound [a]	Solubility / mol·L^{-1} (D_2O)	Log_{10} P_{ow}	Residual starting material (37 °C, 72 h) [b]	
			D_2O ± cosolvent	DMEM-d ± cosolvent
[**2a**]CF_3SO_3	$3.0\cdot10^{-3}$	1.28 ± 0.07	≥ 99 %	≥ 99 %
[**2a**^{Fe}]CF_3SO_3	$3.5\cdot10^{-3}$ [c]	− 0.29 ± 0.03 [c]	93 %	
[**2b**]CF_3SO_3	$2.0\cdot10^{-3}$	1.2 ± 0.1	≥ 99 %	≥ 99 %
[**2b**^{Fe}]CF_3SO_3	$2.6\cdot10^{-3}$ [c]	− 0.17 ± 0.01 [c]	92 %	
[**2c**]CF_3SO_3 [d]	≈ $3\cdot10^{-4}$	≈ 1.7	≥ 99 %	≥ 99 %
[**2c**^{Fe}]CF_3SO_3	$1.5\cdot10^{-3}$ [c]	+ 0.41 ± 0.02 [c]	97 %	

[**2d**]CF_3SO_3	< $3\cdot10^{-4}$ [e]	> 2 [e]	≥ 99 %	≥ 99 %
[**2d^{Fe}**]CF_3SO_3	≈ $3\cdot10^{-4}$ [c]	+ 0.77 ± 0.06 [c]	78 % [c]	88 % [c]

[a] Data is referred collectively to all isomers. [b] In CD_3OD/D_2O 2:1 *V*/*V* for [**2d**]$^+$; D_2O/CD_3OD 1:1 *V*/*V* for [**2c**]$^+$, [**2d^{Fe}**]$^+$; D_2O/CD_3OD 2:1 *V*/*V* for [**2b**]$^+$, [**2c^{Fe}**]$^+$; D_2O for [**2a**]$^+$, [**2a,b^{Fe}**]$^+$. [c] Data taken from the literature.[39,40] [d] In admixture with ≈ 9 % [**4**]CF_3SO_3, which is also unaffected by the thermal treatment (≥ 99 % with respect to the starting material). [e] Beyond the quantitation range.

2.3 Biological studies.

The in vitro cytotoxicity of the novel diruthenium μ-vinyliminium compounds [**2a-d**]CF_3SO_3 was assessed on HT-29 (human colon colorectal adenocarcinoma) and MRC-5 (human embryonic lung) cell lines over a 48 h period. Additionally, the homologous diiron compounds [**2a-d^{Fe}**]CF_3SO_3 and cisplatin as a metal drug reference were included in the study for comparative purposes. The diiron complexes [**2a-d^{Fe}**]$^+$ were previously demonstrated to exhibit strong antiproliferative activity towards A2780 and A2780cisR cancer cell lines, together with a considerable cancer cell selectivity with respect to murine embryonic fibroblast as models of noncancer cells (selectivity index = 6-52).[39,40]

The half maximal inhibitory concentration (IC_{50}) was determined using the resazurin assay and the results are presented in Table 2. Generally, the IC_{50} values for diruthenium compounds were significantly lower than those obtained with the corresponding diiron compounds and cisplatin. Unfortunately, the IC_{50} values of both diiron and diruthenium compounds were similar for noncancer cells (MRC-5) and tumor cells (HT-29), indicating a lack of selectivity of our compounds on the selected cell lines. Of high interest, the same trend is observed in the IC_{50} values with respect to the substituents on the vinyliminium ligand for both metal centers ($d < c \leq a < b$). Given that some triflate salts of various cationic metal complexes revealed lack of cytotoxicity in vivo and/or in vitro,[38,59,60] the activity of the examined diruthenium complexes should be attributed solely to the cationic component.

Table 2. IC_{50} values (in μM) obtained after incubation of diiron and diruthenium compounds with HT-29 and MRC-5 cells for 48 h. Values are given as mean ± standard deviation.

Complex	HT-29	MRC-5
[**2a**^{Fe}]CF_3SO_3	13.9 ± 2.8	11.4 ± 2.8
[**2a**]CF_3SO_3	5.0 ± 3.2	2.0 ± 0.5
[**2b**^{Fe}]CF_3SO_3	18.1 ± 3.3	14.5 ± 0.8
[**2b**]CF_3SO_3	10.7 ± 4.0	4.4 ± 0.9
[**2c**^{Fe}]CF_3SO_3	7.2 ± 3.5	7.2 ± 0.6
[**2c**]CF_3SO_3	3.2 ± 1.9	2.0 ± 1.1
[**2d**^{Fe}]CF_3SO_3	8.8 ± 1.1	2.3 ± 1.0
[**2d**]CF_3SO_3	4.4 ± 1.1	0.3 ± 0.3
cisplatin	13.6 ± 2.4	3.1 ± 0.7

It is documented in the literature that metal complexes can interact with cellular redox systems, resulting in an elevation of oxidative stress levels, which may lead to cell damage and death.[61] To investigate and compare the level of intracellular oxidative stress induced by Ru and Fe complexes, we measured the cellular ROS levels of selected compounds in both cancer cells (HT-29) and healthy cells (MRC-5). As shown in Figure 4a, the fluorescence intensity of ROS in HT-29 cells incubated with [**2d**]$^+$ or [**2d**^{Fe}]$^+$ was significantly higher compared to [**2b**]$^+$ or [**2b**^{Fe}]$^+$, apparently as a consequence of the contribution provided by the ferrocenyl group to ROS production. Moreover, it was observed that HT-29 cells incubated with diruthenium complexes, [**2b**]$^+$ and [**2d**]$^+$, generated a greater amount of ROS compared to cells treated with the diiron homologues, [**2b**^{Fe}]$^+$ and [**2d**^{Fe}]$^+$. Similar observations were noted in MRC-5 cells (Figure S28a).

High levels of ROS can lead to oxidative damage within mitochondria, such as oxidative modification of mitochondrial DNA, membrane lipids and proteins, resulting in compromised mitochondrial function.[62,63] To evaluate mitochondrial respiratory function, the oxygen consumption rate (OCR) was measured using a Seahorse XF96 analyzer. Oligomycin, an ATP inhibitor, was utilized to determine the dioxygen consumed for ATP synthesis. Carbonyl cyanide-*p*-trifluoromethoxyphenylhydrazone (FCCP), a mitochondrial uncoupler, induced the highest level of cellular dioxygen consumption, allowing for the determination of the maximum attainable respiratory rate. Additionally, rotenone and antimycin A, electron transport inhibitors, were used to inhibit

mitochondrial respiration, facilitating the assessment of spare respiratory capacity.[64] For HT-29 cells, as shown in Figure 4b, the OCR values of HT-29 cells treated with [**2d**]$^+$ or [**2d^{Fe}**]$^+$ were significantly lower compared to those treated with [**2b**]$^+$ or [**2b^{Fe}**]$^+$. Moreover, Figure 4c shows that [**2b**]$^+$ and [**2d**]$^+$ exhibited a greater reduction in maximal respiration capacity and spare respiration capacity compared to [**2b^{Fe}**]$^+$ and [**2d^{Fe}**]$^+$, indicating a diminished cellular response to increased energy demands and stress. This underscores the higher detrimental impact of the ruthenium species on mitochondria. Similar observations are valid for MRC-5 cells (Figures S28b,c). These observations align with the results obtained from reactive oxygen species (ROS) analysis.

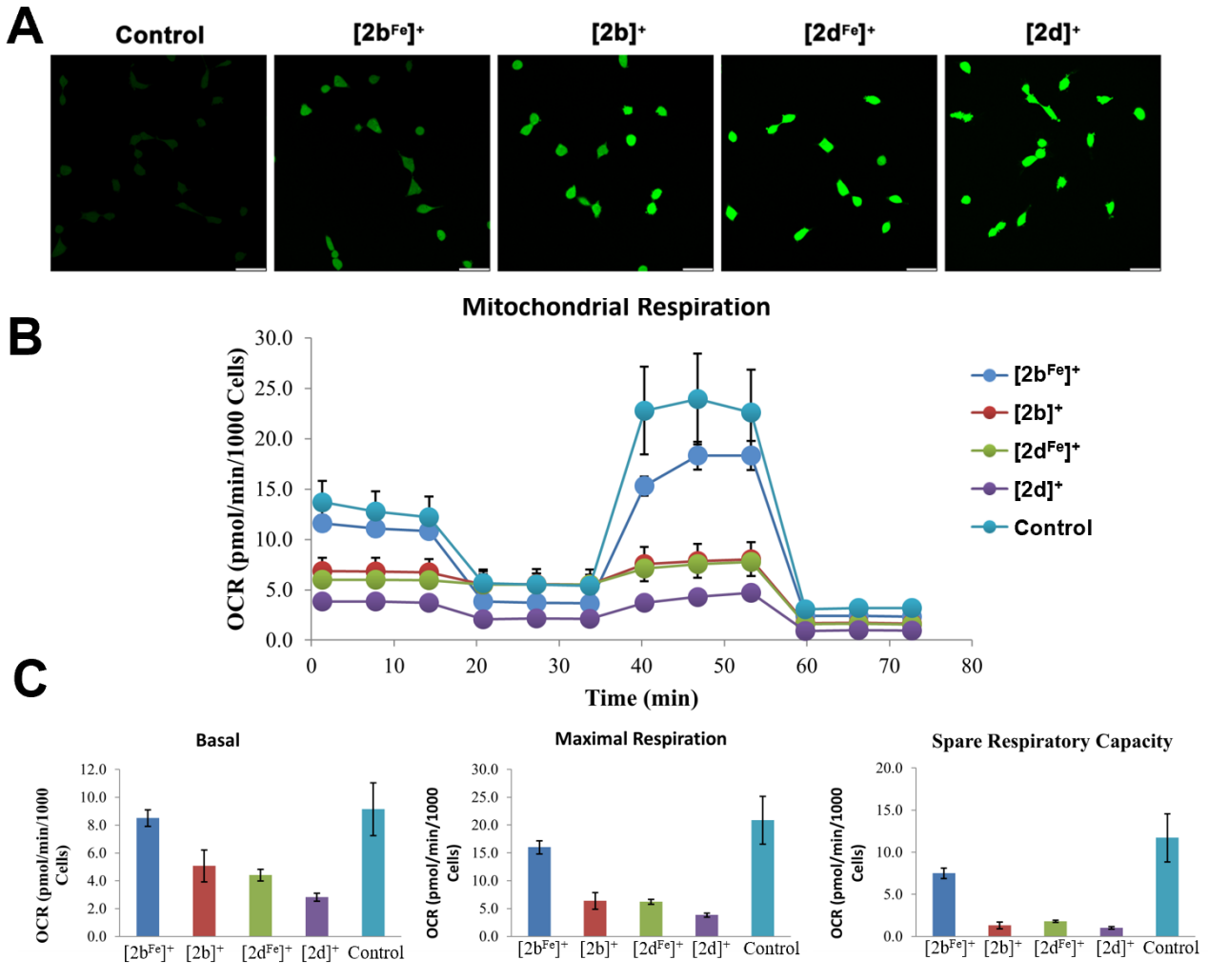

Figure 4. (a) DCFH-DA detection of ROS in HT-29 cells after incubation with compounds for 6 h. $\lambda_{ex}/\lambda_{em}$ = 488/505-530 nm. Scale bars represent 50 μm. (b) Cellular oxygen consumption in HT-29 cells was detected at 24 h after treatment with diruthenium and diiron vinyliminium complexes by Seahorse analyzer (n = 4, mean ± SD). (c) Quantitative comparison of the basal respiration, the maximal respiration and the spare respiratory capacity from (b).

3. Conclusions

Ruthenium complexes have been intensively investigated for their anticancer potential, and most studies have focused on mononuclear Ru^{II} and Ru^{III} species. Here, we report a straightforward one-pot procedure for synthesizing dinuclear ruthenium(I)[65,66] complexes through the incorporation of alkynes within a bridging vinyliminium ligand. The resulting complexes exhibit an exceptional stability in physiological-like solutions and exert a potent antiproliferative activity against the HT-29 cancer cell line, albeit lacking selectivity compared to the MRC-5 non-cancerous cell line. The in vitro activity surpasses that of homologous diiron complexes and is associated with increased ROS production and disruption of mitochondrial metabolism. These features are enhanced by the presence of a ferrocenyl moiety on the vinyliminium ligand, presumably due to the unique redox activity associated with this fragment,[67] consistent with the observed ability of the related complex to disrupt cellular redox homeostasis. Overall, our findings underscore the promising potential of diruthenium bis-cyclopentadienyl complexes in anticancer drug development. Specifically, the construction of vinyliminium ligands provides a convenient platform for incorporating a diversity of organic moieties allowing for the modulation of physicochemical properties and biological activity. Remarkably, the bridging vinyliminium ligand offers broader structural variability, higher robustness and more potent cytotoxicity, compare to related complexes based on the $Ru_2Cp_2(CO)_3$ core featuring different bridging hydrocarbyl ligands.[35,36] Ongoing efforts are devoted to a comprehensive structure-activity investigation, aimed at identifying the best vinyliminium substituent groups.

4. Experimental.

4.1 General experimental details.

Organic reactants and solvents were obtained from TCI Chemicals, Merck, Carlo Erba. Compounds [**1**]CF_3SO_3[47] and [**2a-d^{Fe}**]CF_3SO_3[39,40] were prepared according to the literature. Reactions were carried out under a nitrogen atmosphere using standard Schlenk techniques and solvents deaerated by bubbling argon for 30 minutes. The conversion was monitored by IR spectroscopy. Chromatographic

separations were carried out in air on columns of deactivated neutral alumina (Merck, 4 % *w/w* water). The products were isolated as air- and moisture-stable powders. IR spectra of solids (650-4000 cm^{-1}) were carried out on a Perkin Elmer spectrum One instrument equipped with a U-ATR accessory (ZnSe crystal). IR spectra of solutions were recorded on a Perkin Elmer Spectrum 100 FT-IR spectrometer with a CaF_2 liquid transmission cell (1500-2300 cm^{-1}). UV-Vis spectra (250-800 nm) were recorded on an Ultraspec 2000 spectrophotometer using 10 mm PMMA cuvettes. IR and UV-Vis spectra were processed with Spectragryph.[68] NMR spectra were recorded on a Jeol JNM-ECZ 400 MHz instrument equipped with Royal HFX Broadband probes. Chemical shifts (ppm) are referenced to the residual solvent peaks[69] (^1H, ^{13}C) or to external standards (^{19}F to $CFCl_3$).[70] ^1H and ^{13}C spectra were assigned with the support of ^1H NOESY (mix time 750 ms, relaxation time 1 sec, linewidth 15 Hz) and/or ^1H-^{13}C *gs*-HSQC experiments. NMR signals due to minor diastereoisomers are italicized. Elemental (CNHS) analyses were performed on a Vario MICRO cube instrument (Elementar). ESI-Q/ToF flow injection analyses (FIA) were carried out using a 1200 Infinity HPLC (Agilent Technologies, USA) coupled to a Jet Stream ESI interface (Agilent) with a Quadrupole-Time of Flight tandem mass spectrometer 6530 Infinity Q-TOF (Agilent Technologies). Ca. 1 mg of sample was weighted and dissolved in 1 mL acetonitrile (LC-MS grade, Carlo Erba, Italy) and then further diluted to obtain a 10 ppm solution. Injection volume: 0.1 μL. The flow rate was 0.2 mL/min (total run time 3 min). The ESI operating conditions were: *drying gas* (N_2, purity >98%): 350 °C and 10 L/min; *capillary voltage* 4.5 KV; nozzle voltage: 1 KV; *nebuliser gas* 35 psig; *sheath gas* (N_2, purity >98%): 375 °C and 11 L/min. The fragmentor was kept at 50 V, the skimmer at 65 V and the OCT 1 RF at 750 V. High resolution MS spectra were achieved in positive mode in the range 100-1700 m/z; the mass axis was calibrated daily using the Agilent tuning mix HP0321 (Agilent Technologies) prepared in acetonitrile and water. No uncommon hazards are noted.

$[Ru_2Cp_2(CO)(MeCN)(\mu\text{-}CO)\{\mu\text{-}CNMe(C_6H_{11})\}]CF_3SO_3$, [1-NCMe]$CF_3SO_3$ (Chart 1).

Chart 1. Structure of [**1-NCMe**]$^+$ (wavy bonds represent *E*/*Z* isomerism).

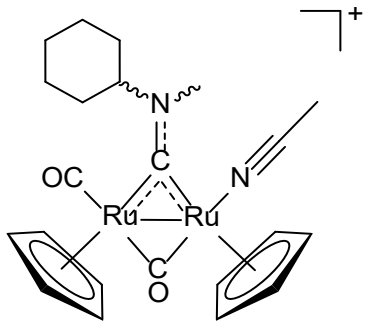

A solution of [**1**]CF_3SO_3 (70 mg, 0.10 mmol), $Me_3NO{\cdot}2H_2O$ (13 mg, 0.12 mmol) in MeCN (5 mL) was stirred at room temperature for 1 h. The resulting yellow solution was taken to dryness under vacuum, affording a yellow-brown solid, containing [**1-NCMe**]CF_3SO_3. IR (CH_2Cl_2 or MeCN): ῡ/cm^{-1} = 1977s (CO), 1811s (μ-CO), 1571m, 1552m (μ-CN). ^{1}H NMR ($CDCl_3$): δ/ppm = *5.44*, 5.35 (s, 5H, Cp); 5.26, *5.21* (s, 5H, Cp'); *4.80*, 4.56 (tt, $^3J_{HH}$ = 12.0, 3.6 Hz, NCH^{Cy}); 3.96, *3.83* (s, 3H, NCH_3); 2.15, *2.13* (s, 3H, CCH_3); 2.06 (d, *J* = 13.5 Hz), 1.99–1.81 (m), 1.81–1.74 (m), 1.55–1.33 (m), 1.31–1.19 (m) (10H, CH_2^{Cy}); *cis-E/cis-Z* ratio = 2.0. Solutions of [**1-NCMe**]CF_3SO_3 in MeCN, THF or MeOH progressively darkened on exposure to ambient air, with formation of a black solid and the appearance of 1770 cm^{-1} absorption in the IR spectrum of the solution (CH_2Cl_2).

Synthesis of diruthenium vinyliminium complexes.

1) *Two step procedure via [**1-NCMe**]*$^+$. A solution of [**1-NCMe**]CF_3SO_3 (≈ 0.1 mmol), freshly prepared from [**1**] CF_3SO_3, $Me_3NO{\cdot}2H_2O$ and MeCN, in CH_2Cl_2, THF or MeOH (6-10 mL) was treated with phenylacetylene (2.0 eq) and stirred at room or reflux temperature for *ca*. 6 hours. Volatiles were removed under vacuum and the residue was moved on top of an alumina column. An orange-brown band was eluted with THF then an orange band was eluted with MeCN. Volatiles were removed under vacuum and the residues were analyzed by IR (CH_2Cl_2) and ^{1}H NMR analyses ($CDCl_3$). Brown solid: **3** + other impurities. Orange solid: [**2c**]CF_3SO_3 + [**1-NCMe**]CF_3SO_3 (THF, room T: 12 %, reflux T: 41 %; CH_2Cl_2, room T: 15 %; MeOH, room T: 19 %) + minor impurities. Related reactions were carried out with propyne or 2-butyne (5.0 eq) in CH_2Cl_2 at room temperature for 12-24 h. An orange band, containing **3**, was eluted with THF. Next, a MeCN/THF 1:2 *V*/*V* mixture

during alumina chromatography allowed to collect a brown band. Propyne: [**2a**]CF_3SO_3 + [**1-NCMe**]CF_3SO_3 (15 %); 2-butyne: [**2b**]CF_3SO_3 + [**1-NCMe**]CF_3SO_3 (52 %).

2) *One-pot method from [1]*$^+$. A solution of [**1**]CF_3SO_3 (70 or 300 mg) and $Me_3NO{\cdot}2H_2O$ (2.0 eq.) in ^{i}PrOH (5 or 8 mL, depending on the amount of [**1**]$^+$) was treated with the appropriate alkyne {2.0 eq. for MeCCH, MeCCMe, PhCCH; 1.2 eq. for FcCCH, Fc = (η^5-C_5H_5)Fe(η^5-C_5H_4))} and stirred at room temperature for 5 h ([**2a-b**]$^+$) or at reflux temperature for 2 h ([**2c-d**]$^+$). Next, volatiles were removed under vacuum and the residue was triturated in a diethyl ether/hexane 1:1 *V*/*V* mixture. The suspension was filtered (G3 sintered glass filter) and the resulting solid ([**2a-d**]CF_3SO_3) was washed with hexane and dried under vacuum (room temperature).

[Ru_2Cp_2(CO)(μ-CO){μ-k*C*,k^3*C*-C^3(Me)C^2HC^1NMe(C_6H_{11})}]CF_3SO_3, [2a]CF_3SO_3 (Chart 2).

Chart 2. Structure of [**2a**]$^+$ (wavy bonds represent *E*/*Z* isomerism; numbering refers to C atoms).

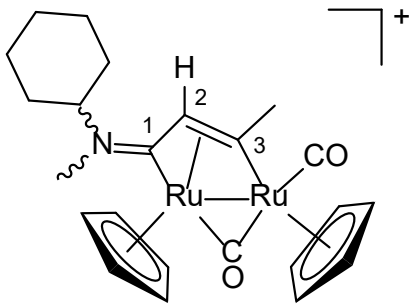

Prepared from [**1**]CF_3SO_3 (70 mg, 0.102 mmol), $Me_3NO{\cdot}2H_2O$ (23 mg, 0.203 mmol) and propyne (≈ 1 mol/L in THF; 0.20 mL, ≈ 0.20 mmol), according to the one-pot procedure. Dark brown solid; yield: 65 mg, 91 %. Soluble in CH_2Cl_2, MeOH, acetone, less soluble in water, insoluble in diethyl ether. Anal. calcd. for $C_{24}H_{28}F_3NO_5Ru_2S$: C, 41.08; H, 4.02; N, 2.00; S, 4.57. Found: C, 40.9; H, 3.94; N, 2.01; S, 4.42. IR (solid state): ῡ/cm^{-1} = 3102w, 2932w, 2857w, 1966s (CO), 1801s (μ-CO); 1663m, 1656m (C^1N); 1560-1540w, 1449w, 1430w, 1410w, 1364w, 1352w, 1272s-sh, 1258s (SO_3), 1222s-sh (SO_3), 1148s (SO_3), 1107w-sh, 1028s, 1013m-sh, 893w, 837m, 826m, 753w, 715w, 692w. IR (CH_2Cl_2): ῡ/cm^{-1} = 1987s (CO), 1816s (μ-CO), 1662m (C^1N), 1552m. ^{1}H NMR (acetone-d_6): δ/ppm = 5.85, *5.84* (s, 5H, Cp); *5.53*, 5.51 (s, 5H, Cp'); *5.38*, 5.29 (s, 1H, C^2H); 4.45, 3.76 (tt, $^3J_{HH}$ =

11.9, 4.0 Hz, NCH^{Cy}); *3.69*, 3.34 (s, 3H, NCH_3); *3.59*, 3.58 (s, 3H, C^3CH_3); 1.92–1.56, 1.51–1.36, 1.32–1.07 (m, 10H, CH_2^{Cy}); *cis-Z*/*cis-E* ratio = 1.1. $^{13}C\{^1H\}$ NMR (acetone-d_6): δ/ppm = 232.5, *231.6* (μ-CO); 216.61, *216.56* (C^1); *199.9*, 199.6 (CO); *187.8*, 187.5 (C^3); 122.4 (q, $^1J_{CF}$ = 322 Hz, CF_3); 93.23, *93.21* (Cp); *89.6*, 89.5 (Cp'); *75.1*, 69.9 (NCH^{Cy}); 59.4, *59.0* (C^2); *43.3*, 40.3 (NCH_3); *42.1*, 41.9 ($C^3\underline{C}H_3$); *31.2*, 30.53, 30.51 (CH_2^{Cy}); 26.0, 25.6, 25.52, 25.47, *25.4* (CH_2^{Cy}). ^{19}F NMR (acetone-d_6): δ/ppm = − 78.7. ^1H NMR ($CDCl_3$): δ/ppm = *5.57*, 5.55 (s, 5H, Cp); 5.45, *5.32** (s, 1H, C^2H); *5.37*, 5.32 (s, 5H, Cp'); 4.28, *3.58* (tt, 1H, $^3J_{HH}$ = 12.0, 3.4 Hz, NCH^{Cy}); 3.56** (s, 3H, C^3CH_3); *3.53*, 3.25 (s, 3H, NCH_3); *2.21–2.13*, 2.10–2.00 (m, 2H, CH_2^{Cy}); 1.86 (m), 1.75 (d, *J* = 13.3 Hz), 1.68–1.55 (m), 1.51–1.35 (m) (8H, CH_2^{Cy}); *cis-Z*/*cis-E* ratio = 1.1. *Hidden by Cp', ** major + minor isomer. Partial (7-15 %) formation of **3** was observed by ^1H NMR in the $CDCl_3$ solution stored at room temperature for several hours. A solution of [**2a**]CF_3SO_3 in isopropanol was heated at reflux temperature for 15 h: no change in the isomer ratio of $[\mathbf{2a}]^+$ was detected by ^1H NMR ($CDCl_3$).

$[Ru_2Cp_2(CO)(\mu\text{-}CO)\{\mu\text{-}\kappa C\text{:}\eta^3\text{-}C^3(Me)C^2(Me)C^1NMe(C_6H_{11})\}]CF_3SO_3$, [2b]$CF_3SO_3$ (Chart 3).

Chart 3. Structure of $[\mathbf{2b}]^+$ (wavy bonds represent *E*/*Z* isomerism; numbering refers to C atoms).

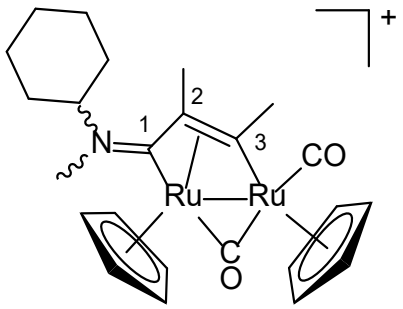

Prepared from [**1**]CF_3SO_3 (70 mg, 0.102 mmol), $Me_3NO{\cdot}2H_2O$ (23 mg, 0.203 mmol) and 2-butyne (16 μL, ≈ 0.205 mmol), according to the one-pot procedure. Dark brown solid; yield: 62 mg, 85 %. Soluble in CH_2Cl_2, MeOH, acetone, less soluble in water, insoluble in diethyl ether. Anal. calcd. for $C_{25}H_{30}F_3NO_5Ru_2S$: C, 41.95; H, 4.23; N, 1.96; S, 4.48. Found: C, 42.1; H, 4.13; N, 1.97; S, 4.22. IR (solid state): ῡ/cm^{-1} = 3100w, 2932w, 2858w, 1963s (CO), 1798s (μ-CO); 1653m, 1648m (C^1N); 1637m-sh, 1560-1540w, 1449w, 1429w, 1411w, 1376w, 1363w, 1351w, 1272s-sh, 1259s (SO_3),

1222s-sh (SO_3), 1149s (SO_3), 1061m, 1028s, 1013m-sh, 998m-sh, 961w, 894w, 824m, 826m, 761w-sh, 753w, 706w, 680w. IR (CH_2Cl_2): $\tilde{\upsilon}$/cm^{-1} = 1984s (CO), 1815s (μ-CO), 1651m (C^1N). ^{1}H NMR ($CDCl_3$): δ/ppm = *5.58*, 5.57 (s, 5H, Cp); 5.34, *5.29* (s, 5H, Cp'); 4.33, 3.44 (tt, $^3J_{HH}$ = 11.9, 3.2 Hz, 1H, NCH^{Cy}); 3.59, *3.14* (s, 3H, NCH_3); 3.50, *3.48* (s, 3H, C^3CH_3); 2.08–2.00, 1.92-1.85 (m, 2H, CH_2^{Cy}); 1.97, *1.95* (s, 3H, C^2CH_3); 1.80–1.61, 1.58–1.35, 1.33–1.07 (m, 8H, CH_2^{Cy}); *cis*-*E*/*cis*-*Z* ratio = 1.1. ^{13}C{^{1}H} NMR ($CDCl_3$): δ/ppm = *232.6*, 231.9 (μ-CO); 217.0, *216.2* (C^1); 199.0, *198.3* (CO); 182.2 (C^3); 121.0 (q, $^1J_{CF}$ = 321 Hz, CF_3); *92.5*, 92.4 (Cp); *89.5*, 89.2 (Cp'); 73.6, *69.1* (NCH^{Cy}); 72.3 (C^2); *40.8*, 39.4 (NCH_3); 38.3, *37.9* ($C^3\underline{C}H_3$); 31.3, *30.5*, *30.1*, 29.7 (CH_2^{Cy}); *25.7*, 25.4, 25.1, *25.0*, *24.9*, 24.8 (CH_2^{Cy}); 17.8, *17.2* ($C^2\underline{C}H_3$). ^{19}F NMR ($CDCl_3$): δ/ppm = − 78.0. Partial (2-20 %) formation of **3** was observed by ^{1}H NMR in the $CDCl_3$ solution stored at room temperature for several hours.

[Ru_2Cp_2(CO)(μ-CO){μ-κ*C*:η^3-C^3(Ph)C^2HC^1NMe(C_6H_{11})}]CF_3SO_3, [2c]CF_3SO_3 (Chart 4).

Chart 4. Structure of [**2c**]$^+$ (wavy bonds represent *E*/*Z* isomerism; numbering refers to C atoms).

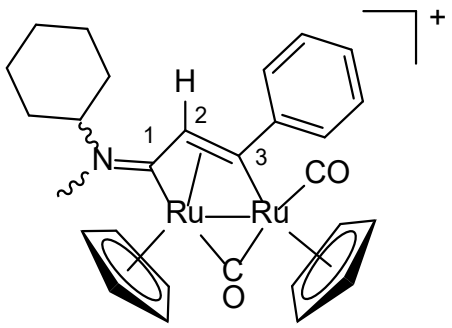

Prepared from [**1**]CF_3SO_3 (70 mg, 0.102 mmol or 300 mg, 0.435 mmol), $Me_3NO{\cdot}2H_2O$ (23 mg, 0.203 mmol or 97 mg, 0.873 mmol) and phenylacetylene (23 μL, 0.209 mmol or 95 μL, 0.865 mmol), according to the one-pot procedure. Red-orange solid, contains *ca*. 9.5 % of [**4**]CF_3SO_3; yield: 70 mg (*ca*. 81 % of [**3**]CF_3SO_3 and 8 % of [**4**]CF_3SO_3) and 330 mg (*ca*. 89 % of [**3**]CF_3SO_3 and 9 % of [**4**]CF_3SO_3). The relative amount of [**4**]CF_3SO_3 in the isolated product of nine different preparations varied within a narrow range (8.3−11 %). The two compounds could not be separated by alumina chromatography. Soluble in DMSO, EtOH, CH_2Cl_2, acetone, THF sparingly soluble in diethyl ether,

water. Anal. calcd. for $(C_{29}H_{30}F_3NO_5Ru_2S)_{0.905}(C_{36}H_{36}F_3NO_4Ru_2S)_{0.095}$: C, 46.11; H, 3.99; N, 1.81; S, 4.14. Found: C, 46.06; H, 3.92; N, 1.85; S, 3.95. IR (solid state): $\tilde{\upsilon}/cm^{-1}$ = 3100w, 3056w-sh, 2931w, 2857w, 1974s (CO), 1805s (μ-CO); 1665m, 1656m (C^1N); 1594w, 1486w, 1449w, 1440w, 1411w, 1352w, 1259s (SO_3), 1222m-sh (SO_3), 1148s (SO_3), 1109w-sh, 1045w-sh, 1028s, 992m-sh, 925w, 893w, 836m, 826m, 765m, 753w-sh, 700m. IR (CH_2Cl_2): $\tilde{\upsilon}/cm^{-1}$ = 1992s (CO), 1820s (μ-CO), 1667w-sh, 1660m (C^1N). IR (THF): $\tilde{\upsilon}/cm^{-1}$ = 1979s (CO), 1813s (μ-CO), 1673m, 1661w-sh (C^1N). ^1H NMR (acetone-d_6): δ/ppm = 7.57 (t, *J* = 7.1 Hz, 2H), 7.42 (t, *J* = 7.5 Hz, 2H), 7.31 (t, *J* = 7.5 Hz, 1H) (Ph); *5.74*, 5.71 (s, 5H, Cp); *5.54*, 5.53 (s, 5H, Cp'); 5.41 (s, 1H, C^2H); 4.56, *3.97* (tt, *J* = 11.9, 3.8 Hz, NCH^{Cy}); *3.79*, 3.47 (s, 3H, NCH_3); *cis-Z*/*cis-E* ratio = 1.2. ^1H NMR ($CDCl_3$): δ/ppm = 7.45–7.29 (m, 5H, Ph); *5.57*, 5.49 (s, 5H, Cp); 5.41, *5.20* (s, 1H, C^2H); *5.30*, 5.25 (s, 5H, Cp'); 4.37, *3.62* (tt, $^3J_{HH}$ = 12.1, 3.8 Hz, NCH^{Cy}); *3.68*, 3.36 (s, 3H, NCH_3); 2.30 (d, *J* = 12.7 Hz), 2.12–1.99, 1.93–1.63, 1.52–1.42, 1.35–1.15 (m) (10H, CH_2^{Cy}); *cis-Z*/*cis-E* ratio = 1.3. $^{13}C\{^1H\}$ NMR ($CDCl_3$): δ/ppm = 231.5, *230.0* (μ-CO); 214.8, *214.5* (C^1); *198.1*, 197.7 (CO); *187.6*, 187.5 (C^3); 154.2 (Ph, C_{ipso}); 128.5, 127.45, 127.39, 127.36 (Ph, C_{para} + C_{meta} + C_{ortho}); 121.0 (q, $^1J_{CF}$ = 320 Hz, CF_3); *93.20*, 93.18 (Cp); *89.6*, 89.3 (Cp'); *75.0*, 69.6 (NCH^{Cy}); 59.5, *59.3* (C^2); 43.4, *40.4* (NCH_3); *30.8*, 30.3, 30.1, *29.8* (CH_2^{Cy}); 25.7, 25.2, 25.1, 25.0, *24.8* (CH_2^{Cy}). ^{19}F NMR ($CDCl_3$): δ/ppm = − 78.0. Minor (2-3 %) formation of **3** was observed by ^1H NMR in the $CDCl_3$ solution stored at room temperature for several hours. A solution of [**2c**]CF_3SO_3 in isopropanol was heated at reflux temperature for 15 h: no change in the isomer ratio of $[\mathbf{2c}]^+$ was detected by ^1H NMR ($CDCl_3$).

$[Ru_2Cp_2(CO)(\mu\text{-}CO)\{\mu\text{-}\kappa C\text{:}\eta^3\text{-}C^3\{(\eta^5\text{-}C_5H_4)FeCp\}C^2HC^1NMe(C_6H_{11})\}]CF_3SO_3$, [2d]$CF_3SO_3$ (Chart 5).

Chart 5. Structure of $[\mathbf{2d}]^+$ (wavy bonds represent *E*/*Z* and *cis*/*trans* isomerism; numbering refers to C atoms).

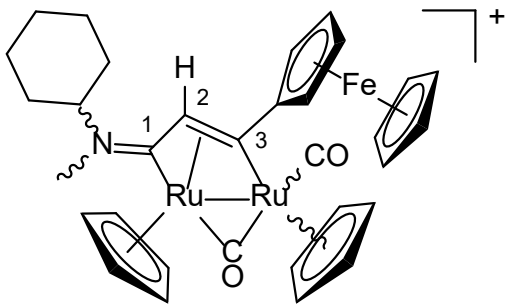

Prepared from [**1**]CF_3SO_3 (70 mg, 0.102 mmol), $Me_3NO{\cdot}2H_2O$ (23 mg, 0.203 mmol) and ethynylferrocene (26 mg, 0.124 mmol), according to the one-pot procedure. Red solid; yield: 79 mg, 89 %. Soluble in DMSO, EtOH, MeOH, acetone, CH_2Cl_2, scarcely soluble in water, insoluble in diethyl ether. X-ray quality crystals of the *cis-E* isomer were obtained from a $CDCl_3$ solution of [**2d**]CF_3SO_3 layered with diethyl ether and settled aside at – 30 °C. Anal. Calcd. For $C_{33}H_{34}F_3FeNO_5Ru_2S$: C, 45.47; H, 3.93; N, 1.61; S, 3.68. Found: C, 45.41; H, 3.87; N, 1.65; S, 3.42. IR (solid state): $\tilde{\upsilon}/cm^{-1}$ = 3095w, 2929w, 2856w, 1967s (CO), 1801s (μ-CO); 1662m, 1655m (C^1N), 1454w, 1449w, 1410w, 1384w, 1350w, 1271s-sh, 1258s (SO_3), 1221m-sh (SO_3), 1148s (SO_3), 1105m, 1208s, 999m-sh, 894w, 835m-sh, 820s, 798m-sh, 786w-sh, 753w, 712w, 683w, 657w. IR (CH_2Cl_2): $\tilde{\upsilon}/cm^{-1}$ = 1988s (CO), 1818s (μ-CO), 1658m (C^1N). ^1H NMR (acetone-d_6): δ/ppm = *5.99*, 5.95 (s, 1H, C^2H); 5.77, *5.74* (s, 5H, CpFeFe); 5.53, *5.49* (s, 5H, Cp'FeFe); *4.58*, 3.90 (tt, $^3J_{HH}$ = 11.9, 3.8 Hz, NCH^{Cy}); 4.51, *4.50*, 4.47, *4.45*, 4.43 (m, 4H, η^5-C_5H_4); *4.28*, 4.26 (s, 5H, $CpFe^{II}$), 3.77, *3.44* (s, 3H, NCH_3); *2.20–2.15*, 2.03–1.98, 1.92–1.60, 1.53–1.41, 1.32–1.18 (m, 10H, CH_2^{Cy}) for *cis-E*/*cis-Z* isomers; 6.40, *6.30* (s, 1H, C^2H); 5.48, *5.44* (s, 5H, CpFeFe); 5.28, *5.27* (s, 5H, Cp'FeFe); 4.34, *4.20* (s, 5H, $CpFe^{II}$); 3.73, *3.60* (s, 3H, NCH_3) for *trans-E*/*Z* isomers; *cis*/*trans* ratio = 19; *cis-E*/*cis-Z* ratio = 1.4. ^1H NMR ($CDCl_3$): δ/ppm = *5.92*, 5.76 (s, 1H, C^2H); 5.55, *5.50* (s, 5H, CpFeFe); 5.32, *5.25* (s, 5H, Cp'FeFe); 4.44, 4.41, 4.36, 4.35, 4.33, 4.29 (m-br, 4H, η^5-C_5H_4); 4.27, 4.21 (s, 5H, $CpFe^{II}$); 3.66, *3.38* (s, 3H, NCH_3); 3.59 (tt, $^3J_{HH}$ = 12.0, 3.4 Hz, NCH^{Cy}); *2.34*, 2.10, 1.94, *1.86* (d, *J* = 13.4 Hz, 2H, CH_2^{Cy}); 1.83–1.58, 1.55–1.34, 1.31–1.10 (m, 8H, CH_2^{Cy}) for *cis-E*/*cis-Z* isomers; 6.40, *6.35* (s, 1H, C^2H); 5.20, *5.18* (s, 5H, CpFeFe); 5.19, *5.15* (s, 5H, Cp'FeFe); *4.25*, 4.25 (s, 5H, $CpFe^{II}$); 3.55, *3.48* (s, 3H, NCH_3) for *trans-E*/*Z* isomers; *cis*/*trans* ratio = 9; *cis-E*/*cis-Z* ratio = 1.4. $^{13}C\{^1H\}$

NMR ($CDCl_3$): δ/ppm = *232.2*, 230.7 (μ-CO); *214.4*, 214.3 (C^1); 198.6, *198.1* (CO); *182.5*, 182.4 (C^3); 121.1 (q, $^1J_{CF}$ = 321 Hz, CF_3); *105.6*, 105.2 ($C^3\underline{C}^{Fc}$); 92.93, 92.91 (CpFeFe); 89.3, 88.9 (Cp'FeFe); 74.8, *68.5* (NCH^{Cy}); 71.5, *71.4* (η^5-C_5H_4); 69.8, 69.7 ($CpFe^{II}$); 69.48, *69.46*, 68.9, *68.8*, 68.4, *68.3* (η^5-C_5H_4); *61.1*, 60.6 (C^2); *43.6*, 40.4 (NCH_3); 30.7, *30.3*, *30.1*, 30.0 (CH_2^{Cy}); *25.8*, 25.3, 25.2, *25.1*, *25.0*, 24.9 (CH_2^{Cy}) for *cis-E*/*cis-Z* isomers; *90.62*, 90.57, 90.5, *90.4* (CpFeFe + Cp'FeFe); *70.3*, 70.2 ($CpFe^{II}$); 59.3 (C^2); 41.2, *39.7* (NCH_3); 31.7, 30.8, 30.4 (CH_2^{Cy}) for *trans-E*/*Z* isomers. ^{19}F NMR ($CDCl_3$): δ/ppm = − 78.0. Minor (2-3 %) formation of **3** was observed by ^1H NMR in the $CDCl_3$ solution stored at room temperature for several hours.

[$Ru_2Cp_2Cl(CO)(\mu\text{-}CO)\{\mu\text{-}CNMe(C_6H_{11})\}$], 3 (Chart 6).

Chart 6. Structure of **3** (wavy bonds represent *E*/*Z* isomerism).

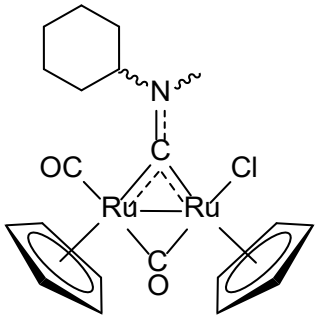

A yellow suspension of [**1**]CF_3SO_3 (70 mg, 0.10 mmol), $Me_3NO{\cdot}2H_2O$ (23 mg, 0.20 mmol) and LiCl (13 mg, 0.31 mmol) in ^{i}PrOH (5 mL) was refluxed under magnetic stirring for 2 h. The resulting red solution was allowed to cool to room temperature and taken to dryness under vacuum. The residue was suspended in a small volume of CH_2Cl_2 and filtered over celite to remove lithium salts. The filtrate was transferred on top of an alumina column (h = 4 cm, d = 3.2 cm). Impurities were eluted with CH_2Cl_2 then an orange band containing the title product was eluted with THF. The eluate was taken to dryness under vacuum and the resulting orange solid was washed with hexane and dried. Yield: 62 mg, 87 %. Soluble in CH_2Cl_2, acetone, insoluble in water and methanol. X-ray quality crystals of **3** were obtained from a $CDCl_3$ solution layered with diethyl ether and settled aside at – 30 °C. Anal. Calcd. for $C_{20}H_{24}ClNO_2Ru_2$: C, 43.84; H, 4.41; N, 2.56. Found: C, 43.65; H, 4.28; N, 2.49.

IR (solid state): ϋ/cm^{-1} = 3095w, 3067w, 2924m, 2854w, 1929s (CO), 1783s (μ-CO), 1569w-sh, 1542m (μ-CN), 1524m-sh, 1507m-sh, 1456w, 1445w, 1429w, 1411w, 1395w, 1347w, 1317w, 1260w, 1250w, 1184w, 1153w, 1105w, 1061m, 1011w, 992w, 916w, 892w, 838m, 800s, 760s. IR (CH_2Cl_2): ϋ/cm^{-1} = 1972s (CO), 1796s (μ-CO), 1545m (μ-CN). ^{1}H NMR ($CDCl_3$): δ/ppm = *5.22*, 5.07 (s, 5H, Cp); *5.11–5.05* (m, hidden by Cp'), 4.68 (tt, *J* = 12.1, 3.4 Hz) (1H, NCH^{Cy}); 5.21, *5.04* (s, 5H, Cp^{Cl}); 3.90, *3.74* (s, 3H, NCH_3); *2.16* (d, *J* = 10.8 Hz), 1.98–1.81 (m) (3H, CH_2^{Cy}); 2.01 (dd, *J* = 15.5, 6.9 Hz, 2H), 1.76 (d, *J* = 12.9 Hz, 1H), 1.67 (qd, *J* = 12.3, 3.7 Hz, 1H), 1.55–1.33 (m, 2H), 1.26–1.16 (m, 1H) (CH_2^{Cy}); *cis-E*/*cis-Z* ratio = 1.3. ^{13}C{^{1}H} NMR ($CDCl_3$) δ/ppm = 305.5, *305.3* (μ-CN); *238.4*, 237.9 (μ-CO); 201.2, *200.9* (CO); *88.6*, 88.5 (Cp); 87.6, *87.5* (Cp^{Cl}); 76.4, *75.0* (NCH^{Cy}); *45.0*, 43.2 (NCH_3); *32.4*, *33.0*, 32.0, 30.7 (CH_2^{Cy}); 26.2, *26.1*, 25.9, *25.52*, *25.48*, 25.4 (CH_2^{Cy}).

[Ru_2Cp_2(CO){μ-κ*C*^{1}:κ*C*^{2}-CH=CPh}{μ-κ*C*:η^3-C^3(Ph)C^2HC^1NMe(C_6H_{11})}]CF_3SO_3, [4]CF_3SO_3 (Chart 7).

Chart 7. Structure of [**4**]$^+$ (numbering refers to C atoms).

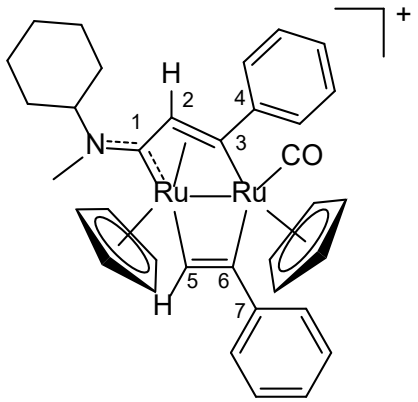

The reaction of [**1**]CF_3SO_3, Me_3NO and phenylacetylene was carried out as described above. The crude reaction mixture, containing [**3c**]CF_3SO_3 and of [**4**]CF_3SO_3 (≈ 9.5:1 ratio) was dissolved in a small volume of THF and moved on top of a dry, solventless neutral alumina column (h 4 cm, d 3.2 cm). The system was kept at room temperature for nine days, with progressive browning of the initial orange-red band. Next, a yellow band was eluted with THF and a bright red band, containing the title product, was eluted with MeCN. Volatiles were removed under vacuum, affording a bright red solid.

Yield: 15 mg, 11 % (with respect to [**1**]$^+$). Preliminary experiments were carried out to establish the change in the relative amount of [**4**]$^+$ with the residence time on alumina: ≈ 10 % (0 h), ≈ 20 % (72 h / 3 days), ≈ 50 % (144 h / 6 days), ≈ 100 % (216 h / 9 days). Attempts to increase the yield of [**4**]$^+$ are described in the ESI. Soluble in CH_2Cl_2, acetone, Et_2O. IR (CH_2Cl_2): $\tilde{\upsilon}$/cm^{-1} = 1996s (CO), 1816w, 1604w, 1480m. ^{1}H NMR ($CDCl_3$): δ/ppm = 7.46–7.37 (m, 7H), 7.33–7.27 (m, 3H) (Ph); 6.61 (s, 1H, C^{5}H); 6.28 (s, 1H, C^{2}H); 5.57 (s, 5H, Cp); 5.34 (s, 5H, Cp'); 4.17–4.06 (m, 1H, NCH^{Cy}); 3.09 (s, 3H, NCH_3); 1.93 (d, J = 13.4 Hz), 1.85–1.64 (m), 1.53–1.22 (m) (CH_2^{Cy}). ^{1}H NMR (acetone-d_6): δ/ppm = 7.71–7.66 (m, 2H), 7.52–7.42 (m, 7H), 7.34–7.28 (m, 1H) (Ph); 6.71 (s, 1H, C^{5}H); 6.56 (s, 1H, C^{2}H); 5.72 (s, 5H, Cp); 5.55 (s, 5H, Cp'); 4.41–4.30 (m, 1H, NCH^{Cy}); 3.25 (s, 3H, NCH_3); 1.92–1.68, 1.59–1.46, 1.34–1.20 (m, CH_2^{Cy}). ^{13}C{^{1}H} NMR (acetone-d_6): δ/ppm = 200.6 (C^1), 193.7 (CO), 182.8 (C^3), 156.0 (C^4), 140.7 (C^7); 130.1, 127.3 (Ph, C_{ortho}); 129.9, 129.8, 128.9, 128.5 (Ph, C_{para} + C_{meta}); 122.5 (d, $^1J_{CF}$ = 322 Hz, CF_3), 110.6 (C^6), 99.7 (C^5), 94.6 (Cp), 84.2 (Cp'), 73.4 (NCH^{Cy}), 68.9 (C^2), 40.9 (NCH_3); 32.0, 26.6, 26.1 (CH_2^{Cy}). ^{19}F NMR (acetone-d_6): δ/ppm = − 78.7. ESI-MS (MeCN): *m/z* = 690.0901 Da; calculated base peak for [**4**]$^+$ ($C_{35}H_{36}NORu_2$): 690.09487 Da.

4.2 X-ray crystallography

Crystal data and collection details for *cis*-*E*-[**2d**]CF_3SO_3 and *cis*-**3** are reported in Table 3. Data were recorded on a Bruker APEX II diffractometer equipped with a PHOTON2 detector using Mo–Kα radiation. The structures were solved by direct methods and refined by full-matrix least-squares based on all data using F^2.[71] Hydrogen atoms were fixed at calculated positions and refined using a riding model. The molecule of *cis*-**3** is disordered and located on a 2-fold axis. Only half of molecule is present in the asymmetric unit of the unit cell and the disorder involves both the terminal CO/Cl ligands and the bridging μ-CO/μ-CNMe(Cy) groups, with 0.5 occupancy factor each. Thus, it is not possible to determine the *E* or *Z* configuration of *cis*-**3**.

Table 3. Crystal data and measurement details for *cis*-*E*-[**2d**]CF_3SO_3 and *cis*-**3**.

	cis-E-[**2d**]CF_3SO_3	*cis*-**3**
Formula	$C_{33}H_{34}F_3FeNO_5Ru_2S$	$C_{20}H_{24}ClNO_2Ru_2$
FW	871.66	547.99
T, K	100(2)	100(2)
λ, Å	0.71073	0.71073
Crystal system	Orthorhombic	Tetragonal
Space group	$P2_12_12_1$	$P4_2/n$
a, Å	12.7653(5)	11.3035(10)
b, Å	12.8075(5)	11.3035(10)
c, Å	19.2917(7)	14.9448(15)
Cell Volume, Å^3	3154.0(2)	1909.5(4)
Z	4	4
D_c, g·cm^{-3}	1.836	1.906
μ, mm^{-1}	1.527	1.736
F(000)	1744	1088
Crystal size, mm	0.16×0.15×0.12	0.21×0.11×0.10
θ limits,°	1.909-25.999	2.259–25.046
Reflections collected	45126	20681
Independent reflections	6213 [R_{int} = 0.0400]	1689 [R_{int} = 0.0631]
Data / restraints /parameters	6213 / 0 / 417	1689 / 247 / 160
Goodness on fit on F^2	1.140	1.428
R_1 ($I > 2\sigma(I)$)	0.0261	0.1266
wR_2 (all data)	0.0611	0.2724
Largest diff. peak and hole, e Å^{-3}	0.768 / –0.451	1.732 / –2.774

4.3 Behavior of diruthenium complexes in aqueous media.

Solubility in water (D_2O). The selected compound was suspended in a D_2O solution (0.7 mL) containing dimethyl sulfone (Me_2SO_2; $1.0\cdot10^{-3}$ mol·L^{-1}) and stirred at room temperature (*ca.* 21 °C) for 2 h. The saturated solution was filtered over celite and analyzed by ^{1}H NMR spectroscopy (delay time = 10 s, number of scans = 20). The concentration (= solubility) was calculated by the relative integral with respect to Me_2SO_2 as internal standard [δ/ppm = 3.12 (s, 6H)].

Octanol-water partition coefficient (Log P_{ow}). Partition coefficients (P_{ow}),[72] were determined by the shake-flask method and UV-Vis measurements, according to a previously described procedure.[30] All operations were carried out at room temperature (*ca*. 21 °C). Stock solutions were prepared in water-saturated octanol for all compounds. The wavelength corresponding to a well-defined absorption of each compound (445-485 nm range) was used for UV-Vis quantitation. The procedure

was repeated three times for each sample (from the same stock solution); results are given as mean ± standard deviation.

Stability assessment in D_2O/CD_3OD at 37 °C. Compounds [**2a**]CF_3SO_3 and [**2a,b^{Fe}**]CF_3SO_3 were dissolved in a D_2O solution containing Me_2SO_2 ($1.0 \cdot 10^{-3}$ mol·L^{-1}; 0.8 mL). Compounds [**2b-d**]CF_3SO_3 and [**2c^{Fe}**]CF_3SO_3 were first dissolved in CD_3OD then diluted with the D_2O/Me_2SO_2 solution (0.8 mL total volume). Methanol was used as a co-solvent to prepare solutions suitable for ^{1}H NMR analysis (> 3 mM); the water/methanol volume ratio (2:1 *V*/*V* for [**2b**]$^+$ and [**2c^{Fe}**]$^+$ 1:1 *V*/*V* for [**2c**]$^+$, 1:2 *V*/*V* for [**2d**]$^+$) was selected with respect to the water solubility of the compound. The solution ($c_{M2} \approx 6 \cdot 10^{-3}$ mol·L^{-1}; M = Fe, Ru) was filtered over celite and analyzed by ^{1}H NMR (delay time = 10 s; number of scans = 20). Next, the solution was heated at 37 °C for 72 h and NMR analyses were repeated. The residual amount of starting material in the final solution was calculated by the relative integral with the internal standard (Me_2SO_2) with respect to the initial spectrum. The isomeric ratios of [**2a-d**]$^+$ are in accordance with those observed in $CDCl_3$ or acetone-d_6 solutions (except the *cis*/*trans* ratio of [**2d**]$^+$) and were unchanged at the end of the thermal treatment. NMR data are reported in the ESI. ^{1}H NMR chemical shifts in D_2O/CD_3OD mixtures are referenced to the Me_2SO_2 peak in pure D_2O [δ/ppm = 3.12 (s, 6H)].

Stability assessment in cell culture medium at 37 °C. Deuterated cell culture medium (DMEM-d) was prepared by dissolving powdered DMEM cell culture medium (1000 mg/L glucose and L-glutamine, without sodium bicarbonate and phenol red; D2902 - Sigma Aldrich) in D_2O (10 mg/mL, according to the manufacturer's instructions). The solution was treated with Me_2SO_2 ($6.3 \cdot 10^{-3}$ mol·L^{-1}) and KH_2PO_4 / Na_2HPO_4 as buffer (25 mM total phosphate, pD = 7.4[73]), then stored at 4 °C under N_2. Solutions of Ru compounds in DMEM-d or DMEM-d/CD_3OD were prepared, treated and analyzed by ^{1}H NMR as previously described. The residual amount of starting material in the final solution resulted ≥ 99 % for all compound tested and no changes in isomeric ratios were detected.

4.4 Biological studies

Cell culture. HT-29 and MRC-5 cells were cultured in McCoy'S 5A and DMEMF-12(Gibco), supplemented with 10 % fetal calf serum (Gibco) and 1% PenStrep (Gibco). Cells were maintained in a humidified atmosphere at 37 °C and 5 % CO_2.

Cytotoxicity. Cells were seeded on 96-well plates at 4000 cells per well and incubated at 37°C for 24 h. Test compounds were prepared in DMSO and sequentially diluted with fresh medium. The concentration of DMSO in the test compound (0.01 µm) was 0.02 %. The old medium was then replaced with fresh medium containing the test compound, after 48 h of incubation, the medium was replaced with 100 µl of fresh medium containing resazurin (0.2 mg/mL). After 4 h incubation, Plates were read with the SpectraMaxM2 Microplate Reader (λ_{exc} = 540 nm; λ_{read} = 590 nm). The concentration effect curves were obtained by GraphPad Prism 8 software. All experiments were performed on triplicate.

ROS measurement. The ROS level was measured using the commercially available dye 2′,7′-dichlorodihydrofluorescein (DCFH-DA). Cells were plated into 8-well plates with a density of $4{\cdot}10^3$ cells per well and allowed to adhere overnight. The medium was replaced by fresh medium containing the diruthenium and diiron vinyliminium complexes (concentration is IC_{50}). After 6 h of incubation, the cells were washed with cold PBS, 20 µM of DCFH-DA are added and incubated in the dark for 30 min. The cells were observed with a confocal microscopy (Ex: 488 nm; Em :505 nm-550 nm).

Cell Mito Stress Test. MRC-5 and HT-29 cells were seeded in Seahorse XFe96 well plates at a density of 10,000 cells /well in 80 µL medium. After 24 h, the medium was replaced with fresh medium and the diruthenium and diiron vinyliminium complexes (concentration were their IC_{50} values) were added. After 24 h of incubation, the regular medium was removed, cells were washed twice using Seahorse Base Media and incubated in a non-CO_2 incubator at 37 °C for 1 h. The oxygen consumption rate (OCR) was measured after sequential addition of oligomycin 10 µM, carbonyl cyanide 4-(trifluoromethoxy) phenylhydrazone (FCCP) 10 µM, rotenone and antimycin A 10 µM). The data were analyzed using the Agilent Seahorse software.

Acknowledgements

L. B. and F. M. thank the University of Pisa for financial support (Fondi di Ateneo 2023) and Prof. Ilaria Degano for HR-MS analysis. This work was financially supported by an ERC Consolidator Grant Photo-MedMet to G. G. (GA 681679). Z. X. thanks the China Scholarship Council for financial support.

Supporting Information Available

IR and NMR spectra; characterization of [**4**]$^+$; NMR data and spectra in aqueous solution; ROS analysis and oxygen consumption in MRC-5 cells. CCDC reference numbers 2338029 ([**2d**]CF_3SO_3) and 2338030 (**3**) contain the supplementary crystallographic data for the X-ray studies reported in this work. These data are available free of charge at http://www.ccdc.cam.ac.uk/structures.

The authors declare no competing financial interests.

References

1 S. Thota, D. A. Rodrigues, D. C. Crans, E. J. Barreiro, Ru(II) Compounds: Next-Generation Anticancer Metallotherapeutics?, J. Med. Chem. 2018, 61, 5805-5821.

2 S. M. Meier-Menches, C. Gerner, W. Berger, C. G. Hartinger, B. K. Keppler, Structure–activity relationships for ruthenium and osmium anticancer agents – towards clinical development, Chem. Soc. Rev., 2018, 47, 909—928.

3 L. Zeng, P. Gupta, Y. Chen, E. Wang, L. Ji, H. Chao, Z.-S. Chen, The development of anticancer ruthenium(II) complexes: from single molecule compounds to nanomaterials, Chem. Soc. Rev., 2017, 46, 5771-5804.

4 B. S. Murray, P. J. Dyson, Recent progress in the development of organometallics for the treatment of cancer. Curr. Opinion Chem. Biol. 2020, 56, 28-34.

5 S. Ghosh, Cisplatin: The first metal based anticancer drug, Bioorg. Chem. 2019, 88, 102925.

6 S. Dilruba, G. V. Kalayda, Platinum-based drugs: past, present and future. Cancer Chemother. Pharmacol. 2016, 77, 1103–1124.

7 M. Marloye, G. Berger, M. Gelbcke, A survey of the mechanisms of action of anticancer transition metal complexes. Future Med. Chem. 2016, 8, 2263-2286.

8 R. Oun, Y. E. Moussa, N. J. Wheate, The side effects of platinum-based chemotherapy drugs: a review for chemists. Dalton Trans. 2018, 47, 6645–6653.

9 P. J. Dyson, Ruthenium – A Non-essential Element that May Become Essential in Treating Chemoresistant Cancers, Chimia 2019, 73, 332–333.

10 Alessio, E. Thirty years of the drug candidate NAMI-A and the myths in the field of ruthenium anticancer compounds: A personal perspective. Eur. J. Inorg. Chem. 2017, 2017, 1549 − 1560.

11 Alessio, E. Thirty years of the drug candidate NAMI-A and the myths in the field of ruthenium anticancer compounds: A personal perspective. Eur. J. Inorg. Chem. 2017, 2017, 1549 − 1560.

12 E. Alessio, L. Messori, NAMI-A and KP1019/1339, Two Iconic Ruthenium Anticancer Drug Candidates Face-to-Face: A Case Story in Medicinal Inorganic Chemistry, Molecules 2019, 24, 1995.

13 R. Trondl, P. Heffeter, C. R. Kowol, M. A. Jakupec, W. Berger, B. K. Keppler, NKP-1339, the fi rst ruthenium-based anticancer drug on the edge to clinical application, Chem. Sci., 2014, 5 , 2925–2932.

14 Pragti, B. Kumar Kundu, S. Mukhopadhyay, Target based chemotherapeutic advancement of ruthenium complexes, Coord. Chem. Rev. 2021, 448, 214169.

15 E. Boros, P. J. Dyson, G. Gasser, Classification of Metal-Based Drugs according to Their Mechanisms of Action. Chem 2020, 6, 41–60.

16 A. A. Nazarov, C. G. Hartinger, P. J. Dyson, Opening the lid on piano-stool complexes: An account of ruthenium(II) e arene complexes with medicinal applications, J. Organomet. Chem. 2014, 751, 251-260.

17 A. Alguacil, F. Scalambra, A. Romerosa, A. Bento-Oliveira, F. Marques, I. Maximiano, R. F. M. de Almeida, A. I. Tomaz, A. Valente, Evaluation of the Antiproliferative Properties of CpRu Complexes Containing N-Methylated Triazaphosphaadamantane Derivatives, Bioinorganic Chemistry and Applications, Volume 2023, Article ID 6669394.

18 Anthony, E. J.; Bolitho, E. M.; Bridgewater, H. E.; Carter, O. W. L.; Donnelly, J. M.; Imberti, C.; Lant, E. C.; Lermyte, F.; Needham, R. J.; Palau, M.; Sadler, P. J.; Shi, H.; Wang, F.-X.; Zhang, W.-Y.; Zhang, Z. Metallodrugs are unique: opportunities and challenges of discovery and development. Chem. Sci. 2020, 11, 12888–12917.

19 Rausch, M.; Dyson, P. J.; Nowak-Sliwinska, P. Recent Considerations in the Application of RAPTA-C for Cancer Treatment and Perspectives for Its Combination with Immunotherapies, Adv. Therap. 2019, 2, 1900042.

20 Weiss, A.; Berndsen, R. H.; Dubois, M.; Müller, C.; Schibli, R.; Griffioen, A. W.; Dyson, P. J.; Nowak-Sliwinska, P. In vivo anti-tumor activity of the organometallic ruthenium(II)-arene complex [Ru(η^6-p-cymene)-Cl_2(pta)] (RAPTA-C) in human ovarian and colorectal carcinomas. Chem. Sci., 2014, 5 , 4742–4748.

21 B. S. Murray, M. V. Babak, C. G. Hartinger, P. J. Dyson, The development of RAPTA compounds for the treatment of tumors, Coord. Chem. Rev. 2016, 306, 86–114.

22 S. Swaminathan, R. Karvembu, Dichloro Ru(II)-p-cymene-1,3,5-triaza-7-phosphaadamantane (RAPTA-C): A Case Study, ACS Pharmacol. Transl. Sci. 2023, 6, 982-996.

23 J. Campos, Bimetallic cooperation across the periodic table, Nat. Rev. Chem. 2020, 4, 696–702.

24 V. Ritleng, M. J. Chetcuti, Hydrocarbyl Ligand Transformations on Heterobimetallic Complexes, Chem. Rev. 2007, 107, 797−858.

25 S. Patra, N. Maity, Recent advances in (hetero)dimetallic systems towards tandem catalysis, Coord. Chem. Rev. 2021, 434, 213803.

26 H. Tsurugi, P. Laskar, K. Yamamoto, K. Mashima, Bonding and structural features of metal-metal bonded homo- and hetero-dinuclear complexes supported by unsaturated hydrocarbon ligands, J. Organomet. Chem.2018, 869, 251-263.

27 G. Bresciani, S. Schoch, L. Biancalana, S. Zacchini, M. Bortoluzzi, G. Pampaloni, F. Marchetti, Cyanide–alkene competition in a diiron complex and isolation of a multisite (cyano)alkylidene–alkene species. Dalton Trans. 2022, 51, 1936-1945.

28 F. Marchetti, Constructing Organometallic Architectures from Aminoalkylidyne Diiron Complexes. Eur. J. Inorg. Chem. 2018, 3987–4003.

29 F. Y. Pétillon, P. Schollhammer, J. Talarmin, Recent advances in the chemistry of tris(thiolato) bridged cyclopentadienyl dimolybdenum complexes, Coord. Chem. Rev. 2017, 331, 73–92.

30 G. Agonigi, L. Biancalana, M. G. Lupo, M. Montopoli, N. Ferri, S. Zacchini, F. Binacchi, T. Biver, B. Campanella, G. Pampaloni, V. Zanotti, F. Marchetti, Exploring the Anticancer Potential of Diiron Bis-cyclopentadienyl Complexes with Bridging Hydrocarbyl Ligands: Behavior in Aqueous Media and In Vitro Cytotoxicity, Organometallics 2020, 39, 645−657.

31 Tolbatov, I.; Barresi, E.; Taliani, S.; La Mendola, D.; Marzo, T.; Marrone, A. Diruthenium(II,III) paddlewheel complexes: effects of bridging and axial ligands on anticancer properties, Inorg. Chem. Front., 2023, 10, 2226-2238

32 Rahman, F.-U.; Zeeshan Bhatti, M.; Ali, A.; Duong, H.-Q.; Zhang, Y.; Ji, X.; Lin, Y.; Wang, H.; Li, Z. T.; Zhang, D.-W. Dimetallic Ru(II) arene complexes appended on bis-salicylaldimine induce cancer cell death and suppress invasion via p53-dependent signaling, Eur. J. Med. Chem. 2018, 157, 1480-1490.

33 Wang, J.; Zhang, Y.; Li, Y.; Li, E.; Ye, W.; Pan, J. Dinuclear Organoruthenium Complex for Mitochondria-Targeted Near-Infrared Imaging and Anticancer Therapy to Overcome Platinum Resistance, Inorg. Chem. 2022, 61, 8267 – 8282.

34 D. Stíbal, B. Therrien, G. Süss-Fink, P. Nowak-Sliwinska, P. J. Dyson, E. Čermáková, M. Řezácová, P. Tomšík, Chlorambucil conjugates of dinuclear p-cymene ruthenium trithiolato complexes: synthesis, characterization and cytotoxicity study in vitro and in vivo, J Biol. Inorg. Chem. 2016, 21, 443–452.

35 G. Bresciani, J. Vančo, T. Funaioli, S. Zacchini, T. Malina, G. Pampaloni, Z. Dvořák, Z. Trávníček, F. Marchetti, Anticancer Potential of Diruthenium Complexes with Bridging Hydrocarbyl Ligands from Bioactive Alkynols, Inorg. Chem. 2023, 62, 15875–15890.

36 G. Bresciani, S. Boni, T. Funaioli, S. Zacchini, G. Pampaloni, N. Busto, T. Biver, F. Marchetti, Adding Diversity to a Diruthenium Biscyclopentadienyl Scaffold via Alkyne Incorporation: Synthesis and Biological Studies, Inorg. Chem. 2023, 62, 12453−12467.

37 L. Biancalana, M. De Franco, G. Ciancaleoni, S. Zacchini, G. Pampaloni, V. Gandin, F. Marchetti, Easily Available, Amphiphilic Diiron Cyclopentadienyl Complexes Exhibit in Vitro Anticancer Activity in 2D and 3D Human Cancer Cells through Redox Modulation Triggered by CO Release, Chem. Eur. J. 2021, 27, 10169–10185.

38 D. Rocco, L. K. Batchelor, G. Agonigi, S. Braccini, F. Chiellini, S. Schoch, T. Biver, T. Funaioli, S. Zacchini, L. Biancalana, M. Ruggeri, G. Pampaloni, P. J. Dyson, F. Marchetti, Anticancer Potential of Diiron Vinyliminium Complexes. Chem. Eur. J. 2019, 25, 14801-14816.

39 Braccini S; Rizzi, L. Biancalana, A. Pratesi, S. Zacchini, G. Pampaloni, F. Chiellini, F. Marchetti, Anticancer Diiron Vinyliminium Complexes: A Structure–Activity Relationship Study. Pharmaceutics 2021, 13, 1158.

40 S. Schoch, S. Braccini, L. Biancalana, A. Pratesi, T. Funaioli, S. Zacchini, G. Pampaloni, F. Chiellini and F. Marchetti, When ferrocene and diiron organometallics meet: triiron vinyliminium complexes exhibit strong cytotoxicity and cancer cell selectivity, Inorg. Chem. Front., 2022, 9, 5118-5139.

41 G. Bresciani, J. Cervinka, H. Kostrhunova, L. Biancalana, M. Bortoluzzi, G. Pampaloni, V. Novohradsky, V. Brabec, F. Marchetti, J. Kasparkova, N-Indolyl diiron vinyliminium complexes exhibit antiproliferative effects in cancer cells associated with disruption of mitochondrial homeostasis, ROS scavenging, and antioxidant activity, Chemi.-Biol. Interact. 2023, 385, 110742

42 B. Campanella, S. Braccini, G. Bresciani, M. De Franco, V. Gandin, F. Chiellini, A. Pratesi, G. Pampaloni, L. Biancalana, F. Marchetti, The choice of μ-vinyliminium ligand substituents is key to optimize the antiproliferative activity of related diiron complexes, Metallomics 2023, 15, mfac096.

43 G. Ciancaleoni, S. Zacchini, V. Zanotti, F. Marchetti, DFT Mechanistic Insights into the Alkyne Insertion Reaction Affording Diiron μ-Vinyliminium Complexes and New Functionalization Pathways. Organometallics 2018, 37, 3718−3731.

44 T. Y. Luh, Trimethylamine N-Oxide-A Versatile Reagent For Organometallic Chemistry. Coord. Chem. Rev. 1984, 60, 255-276.

45 G. Bresciani, S. Zacchini, G. Pampaloni, F. Marchetti, Carbon − Carbon Bond Coupling of Vinyl Molecules with an Allenyl Ligand at a Diruthenium Complex, Organometallics 2022, 41, 1006 − 1014.

46 K. J. Adams, J. J. Barker, S. A. R. Knox, A. G. Orpen, Linking and fragmentation of alkynes at a triruthenium centre, J. Chem. Soc., Dalton Trans., 1996, Pages 975-988.

47 Dyke, A. F.; Knox, S. A. R.; Naish, P. J.; Taylor, G. E. Organic chemistry of dinuclear metal centres. Part 1. Combination of alkynes with carbon monoxide at di-iron and diruthenium centres: crystal structure of $[Ru_2(CO)(\mu\text{-}CO)\{\mu\text{-}\sigma\text{:}\eta^3\text{-}C(O)C_2Ph_2\}(C_5H_5)_2]$. J. Chem. Soc. Dalton Trans. 1982, 1297-1307.

48 J. A. S. Howell, A. J. Rowan, Synthesis and Fluxional Character of Complexes of the Type $[M_2(cp)_2{=}(CO)B(CNR)]$ (M = Fe or Ru), J. Chem. Soc. Dalton Trans. 1980, 503-510.

49 J. N. L. Dennett, S. A. R. Knox, K. M. Anderson, J. P. H. Charmant, A. Guy Orpen, The synthesis of $[FeRu(CO)_2(m\text{-}CO)_2(Cp)(C_5Me_5)]$ and convenient entries to its organometallic chemistry, Dalton Trans. 2005, 63–73.

50 J. Vančo, M. Fiaschi, L. Biancalana, T. Malina, Z. Dvořák, T. Funaioli, S. Zacchini, M. Guelfi, Z. Trávníček, F. Marchetti, An Exceptionally Aqueous Stable Diruthenium N-Indolyl Aminocarbyne Complex as a Prospective Anticancer Drug, Inorg. Chem. Front. 2024, DOI: 10.1039/d4qi00096j.

51 L. Busetto, F. Marchetti, S. Zacchini, V. Zanotti, New diruthenium vinyliminium complexes from the insertion of alkynes into bridging aminocarbynes, J. Organomet. Chem. 2006, 691, 2424–2439

52 F. Althobaiti, H. A. Sahyon, M. M.A.H. Shanab, A. Aldhahrani, M. A. Helal, A. Khireldin, A. Ghany F. Shoair, A. S.A. Almalki, A. M. Fathy, A comparative study of novel ruthenium(III) and iron(III) complexes containing uracil; docking and biological studies, J. Inorg. Biochem. 2023, 247, 112308.

53 According to IUPAC (Red Book, 2005, pages 222-223), the correct description for the coordination mode of the vinyliminium ligand in these dimetal complexes is "μ-1κ*C*^{3}:2(1-3)η-", wherein 1 and 2 represent the metal atom numbering and 1-3 represent the carbon atom numbering. For the sake of simplicity, we will use the notation "μ-κ*C*:η^3" throughout the manuscript.

54 A. F. Dyke, S. A. R. Knox, P. J. Naish, G. E. Taylor, Organic Chemistry of Dinuclear Metal Centres. Part 1. Combination of Alkynes with Carbon Monoxide at Di-iron and Diruthenium Centres: Crystal Structure of $[Ru_2(CO)(\mu\text{-}CO)\{\mu\text{-}\sigma\text{:}\eta^3\text{-}C(O)C_2Ph_2\}(h\text{-}C_5H_5)_2]$, J. Chem. Soc. Dalton Trans 1982, 1297-1307.

55 S. A. R. Knox, K. A. Macpherson, A. Guy Orpen, M. C. Rendle, Organic Chemistry of Dinuclear Metal Centres. Part 13. Synthesis, Structure, and Reactivity of $[Ru_2(CO)_4(\eta^5\text{:}\eta^{5'}\text{-}C_5H_4CH_2C_5H_4)]$, J. Chem. Soc. Dalton Trans 1989, 1807-1813.

56 R. Boese, J. K. Cammack, A. J. Matzger, K. Pflug, W. B. Tolman, K. P. C. Vollhardt, T. W. Weidman, Photochemistry of (Fulvalene)tetracarbonyldiruthenium and Its Derivatives: Efficient Light Energy Storage Devices, J. Am. Chem. Soc. 1997, 119, 6757-6773.

57 M. V. Ovchinnikov, D. P. Klein, I. A. Guzei, M.-G. Choi, R. J. Angelici, Reactions of the Dinuclear Ruthenium Complex $\{(\eta^5\text{-}C_5H_3)_2(SiMe_2)_2\}Ru_2(CO)_4$, Featuring a Doubly Linked Dicyclopentadienyl Ligand, Organometallics 2002, 21, 617-627..

58 D. P. Klein, A. Ellern, R. J. Angelici, New Mechanism for the Intermolecular Hydroamination of Alkynes: Catalysis by Dinuclear Ruthenium Complexes with a Rigid Dicyclopentadienyl Ligand, Organometallics 2004, 23, 5662-5670.

59 O. A. Lenis-Rojas, M. P. Robalo, A. I. Tomaz, A. Carvalho, A. R. Fernandes, F. Marques, M. Folgueira, J. Y. Çez, D. Vazquez-Garcia, M. Ljpez, Torres, A. Fernandez, J. J. Fernandez, RuII(p-cymene) Compounds as Effective and Selective Anticancer Candidates with No Toxicity in Vivo, Inorg. Chem. 2018, 57, 13150–13166.

60 S. Wu, K. Liao, J. Chen, F. Li, Facile synthesis of an acid-responsive cinnamaldehyde-pendant polycarbonate for enhancing the anticancer efficacy of etoposide via glutathione depletion, RSC Adv., 2024, 14, 15365-15373.

61 J. Kim, A. Park, J. Hwang, X. Zhao, J. Kwak, H. W. Kim, M. Ku, J. Yang, T. Il Kim, K.-S. Jeong, U. Choi, H. Lee, S. J. Shin, KS10076, a chelator for redox-active metal ions, induces ROS-mediated STAT3 degradation in autophagic celldeath and eliminates ALDH1+ stem cells, Cell Reports 2022, 40, 111077.

62 A, Banstola, K. Poudel, S. Pathak, P. Shrestha, J. O. Kim, J.-H. Jeong, S. Yook, Hypoxia-Mediated ROS Amplification Triggers Mitochondria-Mediated Apoptotic Cell Death via PD-L1/ROS-Responsive, Dual-Targeted, Drug-Laden Thioketal Nanoparticles, ACS Appl. Mater. Interfaces 2021, 13, 19, 22955–22969.

63 X. Luo, X. Gong, L. Su, H. Lin, Z. Yang, X. Yan, J. Gao, Activatable Mitochondria-Targeting Organoarsenic Prodrugs for Bioenergetic Cancer Therapy, Angew. Chem. Int. Ed. 2021, 60, 1403-1410.

64 S. Kumar, M. Jones, Q. Li, D. B. Lombard, Assessment of Cellular Bioenergetics in Mouse Hematopoietic Stem and Primitive Progenitor Cells using the Extracellular Flux Analyzer, J Vis Exp. 2021, 175, e63045.

65 Both the aminocarbyne precursors, **1**, and alkylidene derivatives (not reported here), which can be obtained by nucleophilic additions to the vinyliminium ligand, unequivocally feature ruthenium(I). Therefore, although the vinyliminium ligand can be described in terms of different resonance forms, wherein the oxidation state of the metal centers apparently fluctuates from +I to +II [28, 66], we argue that designating the ruthenium oxidation state as +I offers the most chemically sensible depiction.

66 L. Biancalana, F. Marchetti, Aminocarbyne ligands in organometallic chemistry, Coord. Chem. Rev. 2021, 449, 214203.

67 B. Sharma, V. Kumar, Has Ferrocene Really Delivered Its Role in Accentuating the Bioactivity of Organic Scaffolds?, J. Med. Chem. 2021, 64, 16865 – 16921.

68 F. Menges, "Spectragryph - optical spectroscopy software", Version 1.2.16.1, @ 2016-2022, https://www.effemm2.de/spectragryph/.

69 G. R. Fulmer, A. J. M. Miller, N. H. Sherden, H. E. Gottlieb, A. Nudelman, B. M. Stoltz, J. E. Bercaw, K. I. Goldberg, NMR Chemical Shifts of Trace Impurities: Common Laboratory Solvents, Organics, and Gases in Deuterated Solvents Relevant to the Organometallic Chemist, Organometallics 2010, 29, 2176–2179.

70 R. K. Harris, E. D. Becker, S. M. Cabral De Menezes, R. Goodfellow, P. Granger, NMR nomenclature. Nuclear spin properties and conventions for chemical shifts (IUPAC Recommendations 2001), Pure Appl. Chem. 2001, 73, 1795–1818.

71 Sheldrick, G. M. Crystal structure refinement with SHELXL. Acta Crystallogr. C2015, 71, 3-8.

72 Defined as $P_{ow} = c_{org}/c_{aq}$, where c_{org} and c_{aq} are the molar concentrations of the selected compound in the n-octanol and aqueous phase, respectively. (a) OECD Guidelines for Testing of Chemicals. In OECD, Paris: 1995; Vol. 107; (b) J. C. Dearden and G. M. Bresnen, *Quant. Struct.-Act. Relat.* 1988, **7**, 133-144.

73 Calculated by the formula pD = pH* + 0.4, where pH* is the value measured for H_2O-calibrated pH-meter; (a) C. C. Westcott, pH Measurements; Academic Press: New York, 1978; (b) A. K. Covington, M. Paabo, R. A. Robinson, R. G. Bates. Anal. Chem. 1968, 40, 700-706.